A multifluid-PBE model for simulation of mass transfer limited processes operated in bubble columns

Camilla Berge Vik, Jannike Solsvik, Magne Hillestad, Hugo A. Jakobsen

Department of Chemical Engineering, Norwegian University of Science and Technology (NTNU), N-7491 Trondheim, Norway

Abstract

Modeling of reactive dispersed flows with interfacial mass transfer limitations require an accurate description of the interfacial area, mass transfer coefficient and the driving force. The driving force is given by the difference in species composition between the continuous and dispersed phases and thus depends on bubble size. This paper shows the extension of the multifluid-PBE model to reactive and non-isothermal flows with novel transport equations for species mass and temperature which are continuous functions of bubble size. The model is demonstrated by simulating the Fischer-Tropsch synthesis operated in a slurry bubble column at industrial conditions. The simulation results show different composition and velocity for the smallest and largest bubbles. The temperature profile was independent on bubble size due to efficient heat exchange. The proposed model is particularly useful in investigating the effects of bubble size on strongly mass transfer limited processes

Email addresses: camilla.berge.vik@ntnu.no (Camilla Berge Vik), jannike.solsvik@ntnu.no (Jannike Solsvik), magne.hillestad@ntnu.no (Magne Hillestad), hugo.a.jakobsen@ntnu.no (Hugo A. Jakobsen)

operated in the heterogeneous flow regime.

Keywords: kinetic theory of granular flow, multifluid model, population balance equation, dispersed phase flow, Fischer-Tropsch, bubble column

---

1. Introduction

1.1. Interfacial Mass Transfer Limited Processes

For interfacial mass transfer limited processes the interfacial mass transport phenomena are limiting the overall reaction rate and thus the efficiency of the process. A typical example is bubble columns where gas is injected into the reactor and forms gas bubbles. The gaseous reactants must be transported out of the gas bubbles and into the bulk liquid phase in order to be converted to products.

For interfacial mass transfer limited processes the mass transfer through the liquid film surrounding the bubble is generally the limiting step, as the diffusion coefficient in a liquid is much smaller than in a gas. The mass transfer of species s from the bubble to the bulk liquid can then be modeled as (e.g. Jakobsen (2014)):

$$\Gamma_s = a_L k_{L,s} \rho_L (\omega^*_{L,s} - \omega_{L,s}) \tag{1}$$

where a_L is the gas-liquid interfacial area, $k_{L,s}$ the mass transfer coefficient, $\omega^*_{L,s}$ the weight fraction of species s at the interface and $\omega_{L,s}$ the concentration of s in the bulk liquid. A proper description of mass transfer thus relies on:

- An accurate description of the gas-liquid interfacial area a_L,

- an accurate description of the driving force for mass transfer (here: $\omega^*_{L,s} - \omega_{L,s}$))
- and an accurate parameterization of the mass transfer coefficient $k_{L,s}$.

The driving force for the interfacial mass transfer flux is generally related to the difference in composition in the two phases. In this work the gas composition is considered a function of bubble size. This means that the driving force for mass transfer is a function of bubble size – whether considering the overall mass transfer resistance or simplifying using only the liquid resistance as in Eq. (1).

1.2. Multifluid Models

In general, there are two main frameworks available for deriving the transport equations for mass, species mass, momentum and energy for multiphase flows; continuum mechanics (CM) and statistical mechanics (SM) (Solsvik and Jakobsen, 2016). The multifluid model, derived in the framework of CM is the most common (Jakobsen, 2014). However, this model falls short in describing the interfacial area a_L of dispersed flows. Unless one is performing direct numerical simulations, some type of averaging is required and as a consequence the information about the bubble size and thus interfacial area is lost. One approach to reconstruct the interfacial area is to complement the dispersed phase equations with a population balance equation (PBE). The model is then termed a combined multifluid-PBE model.

1.3. The PBE

The PBE keeps track of the number of bubbles and their size and can also account for breakage and coalescence events. Its derivation is provided both in the CM framework

by Randolph (1964), Randolph and Larson (1988) and Ramkrishna (2000) and in the SM framework by e.g. Williams (1958) and Hulburt and Katz (1964). A recent review on the foundation of PBE and its derivation is given by Solsvik and Jakobsen (2014b).

1.3.1. The sectional PBE

In common CFD software packages such as ANSYS CFX the PBE is added to the Reynolds averaged transport equations derived from CM. The dispersed phase is then divided into a number of bubble classes i and a discrete form of the number density is solved for. When all bubbles have the same velocity this model is called the *homogeneous-MUSIG model* (Lo, 1996). Advancing the model to allow for different bubble velocities (typically three bubble size classes) it is termed the *inhomogeneous-MUSIG model* (Krepper et al., 2008). In this approach the number density function is an output variable - with a resolution corresponding to the number of size classes.

1.3.2. The moment form of the PBE

To save computation time, some integrate the PBE over the entire size space to obtain a set of moment equations and solve for these instead. Typically only three moments of the distribution are computed. This approach is described in e.g. the textbook by Marchisio and Fox (2013). The number density function itself is lost in this procedure, i.e. it is no longer an output variable.

1.3.3. The continuous PBE

Instead of using the CM framework, the equations of change for the bubbly flow can be derived through the SM, in particular kinetic theory of granular flow (KTGF) as shown by Dorao (2006); Nayak et al. (2011); Patruno (2010); Solsvik and Jakobsen (2014a). The bubbles are then described as a granular flow, which on the particle (granule, or here: bubble) level is governed by a Boltzmann-like equation. Moments are formed of the Boltzmann-like equation to calculate average fluid properties such as velocity, mass density, composition and temperature. Equations of change as continuous functions of space, time and bubble size are then obtained, where the PBE is one of the equations. Using spectral or spectral-element methods one can solve for a continuous mass density function and calculate the necessary moments such as interfacial area a_L and Sauter mean diameter as a simple post-processing procedure. This approach results in a continuous PBE, in contrast to a sequential PBE (the MUSIG models) and the moment form of the PBE. The distinction between these three is illustrated in Figure 1. The contrast between the MUSIG and the continuous multifluid-PBE models is illustrated in Figure 2.

1.4. This work and highlighting novelty

Both the MUSIG and moment methods address the issue of an accurate prediction of the interfacial area a_L, taking breakage and coalescence into account. The inhomogeneous-MUSIG model also to some extent lets the bubbles have different velocities and thus accounts for the fact that bubbles have different residence times depending on their size. However, a crucial point for mass transfer limited processes

is not addressed by the MUSIG and moment methods: the accurate prediction of the driving force for mass transfer in the case of reactive dispersed flow.

For a reactive system with interfacial mass transfer limitations the gas concentration of species s is likely to be different for bubbles of different size. Smaller bubbles change composition faster as they have a larger surface area per volume. Different mass transfer fluxes for different sized bubbles is a known issue (e.g. de Swart et al. (1996)), and may be counteracted by e.g. ensuring small enough bubbles by additional distributor plates along the height of the reactor (Jakobsen, 2014) or by cutting the bubbles using a wire mesh (Segers, 2015). A model to describe this bubble size dependency of the composition for dispersed reactive flows and subsequently the driving force for mass transfer is not found in the literature. A novel model in this category is thus proposed in this paper.

1.4.1. The continuous multifluid-PBE model is extended to reactive flows

Based on the works by Reyes (1989), Lafi and Reyes (1994), Lathouwers and Bellan (2000) and Chao (2012) we extend the continuous multifluid-PBE model by Dorao (2006); Nayak et al. (2011); Patruno (2010); Solsvik and Jakobsen (2014a) to reactive and non-isothermal flows. The novelty is thus that we derive equations of change also for weight fractions (species mass) as continuous functions of bubble size. In other words, the proposed model lets the weight fractions differ not only for different positions in the reactor, but also for different sized bubbles. This addresses the issue of a more accurate description of the driving force for mass transfer – through the inclusion of bubble size.

1.4.2. The continuous multifluid-PBE model is extended to non-isothermal flows

Similarly the bubbles are allowed to have different temperatures based on their size. Cooling and heating are important mechanisms in chemical reactors, in particular in reactive systems where temperature limitations are strict (e.g. biological processes). With a bubble size dependent temperature one can get information on whether all different sizes of bubbles are within a temperature criteria rather than just the average. Typical profiles provided by the proposed model are shown in Figure 3, where the size dependent weight fractions and temperature are novel profiles.

1.4.3. All dispersed phase equations are derived through the same theoretical framework: KTGF

In combination with the previously derived bubble size dependent velocity and mass density a complete dispersed phase model is derived within a unified framework; KTGF. A derivation of the entire model for the dispersed phase through one and the same theoretical framework is an advantage due to consistency. Similar averaging procedures performed for all transport equations are desirable from a theoretical point of view.

1.4.4. The proposed model is demonstrated on the Fischer-Tropsch synthesis

To illustrate the capabilities of the proposed model it is demonstrated on the Fischer-Tropsch synthesis (FTS) in a slurry bubble column (SBC) operating at industrial conditions. Reactor dimensions and operating conditions are found in Table 1. The dispersed phase equations are cross-sectionally averaged and combined with the con-

ventional CM equations for the continuous phase presented in Vik et al. (2015). The resultant model is implemented in MATLAB® and solved using orthogonal collocation, described in e.g. Solsvik and Jakobsen (2013).

1.5. Paper outline

The model derivation is given in Section 2. Selected closures are given in Section 3. A discussion of the model is found in Section 2.4. The model capabilities are demonstrated briefly in Section 4. Concluding remarks are given in Section 5.

2. Model derivation

In this section the equations of change for mass, species mass, momentum and energy for a reactive multiphase disperse system are derived. The necessary theory is outlined in the textbook by Jakobsen (2014) and in the works by Dorao (2006); Lathouwers and Bellan (2001); Nayak et al. (2011); Patruno (2010); Solsvik and Jakobsen (2014a) and Chao (2012).

2.1. Definitions

The starting point is a time dependent microscopical number density function

$$p = p(\boldsymbol{r}, \xi, \boldsymbol{c}, \Xi, \omega_{s,p}, T_p, m_p, t) \tag{2}$$

describing the number density of bubbles of size ξ, weight fraction of component s $\omega_{s,p}$, temperature T_p, mass m_p with velocity $\boldsymbol{c}$ and growth velocity Ξ at position $\boldsymbol{r}$

at time t. $\boldsymbol{r}$ and $[\xi, \omega_{s,p}, T_p, m_p]$ are the coordinates in physical space and property space, respectively. Together they form the phase space for the particle. $\boldsymbol{c}$ and Ξ represent the microscopical velocities in physical space and size. We define an *average* number density function $f(\boldsymbol{r}, \xi, t)$ by integrating over all velocities, temperature, weight fractions and the particle mass, but not over the particle size ξ:

$$f(\boldsymbol{r}, \xi, t) = \int_{-\infty}^{+\infty} p(\boldsymbol{r}, \xi, \boldsymbol{c}, \Xi, \omega_{s,p}, T_p, m_p, t) \, \mathrm{d}\boldsymbol{c} \, \mathrm{d}\Xi \, \mathrm{d}\omega_{s,p} \, \mathrm{d}T_p \, \mathrm{d}m_p \tag{3}$$

Correspondingly, we define an average mass density function $f_d(\boldsymbol{r}, \xi, t)$ by multiplying with the microscopical mass m_p and integrating over all velocities, temperature, weight fractions and the particle mass, but not over the particle size ξ:

$$f_d(\boldsymbol{r}, \xi, t) = \int_{-\infty}^{+\infty} m_p p(\boldsymbol{r}, \xi, \boldsymbol{c}, \Xi, \omega_{s,p}, T_p, m_p, t) \, \mathrm{d}\boldsymbol{c} \, \mathrm{d}\Xi \, \mathrm{d}\omega_{s,p} \, \mathrm{d}T_p \, \mathrm{d}m_p \tag{4}$$

$f_d(\boldsymbol{r}, \xi, t)$ and $f(\boldsymbol{r}, \xi, t)$ are momenta of the microscopical number density p. In general, momenta of the microscopical density function p are applied in KTG and KTGF to describe the average fluid properties by integrating over all microscopical velocities. The moment is denoted $\langle \psi_p \rangle$ where ψ_p is a microscopical (particle) quantity:

$$\langle \psi_p \rangle = \int_{-\infty}^{+\infty} \psi_p m_p P(\boldsymbol{r}, \xi, \boldsymbol{c}, \Xi, \omega_{s,p}, T_p, m_p, t) \, \mathrm{d}\boldsymbol{c} \, \mathrm{d}\Xi \, \mathrm{d}\omega_{s,p} \, \mathrm{d}T_p \, \mathrm{d}m_p \tag{5}$$

where $P(\boldsymbol{r}, \xi, \boldsymbol{c}, \Xi, \omega_{s,p}, T_p, m_p, t)$ is a normalized microscopical number density function defined as:

$$P(\boldsymbol{r}, \xi, \boldsymbol{c}, \Xi, \omega_{s,p}, T_p, m_p, t) = \frac{p(\boldsymbol{r}, \xi, \boldsymbol{c}, \Xi, \omega_{s,p}, T_p, m_p, t)}{f_d(\boldsymbol{r}, \xi, t)} \tag{6}$$

This yields an alternative formulation of the moment in terms of the mass density function:

$$\begin{aligned} \langle \psi_p \rangle &= \int_{-\infty}^{+\infty} \psi_p m_p \frac{p(\boldsymbol{r}, \xi, \boldsymbol{c}, \Xi, \omega_{s,p}, T_p, m_p, t)}{f_d(\boldsymbol{r}, \xi, t)} \, \mathrm{d}\boldsymbol{c} \, \mathrm{d}\Xi \, \mathrm{d}\omega_{s,p} \, \mathrm{d}T_p \, \mathrm{d}m_p \\ &= \frac{1}{f_d(\boldsymbol{r}, \xi, t)} \int_{-\infty}^{+\infty} \psi_p m_p p(\boldsymbol{r}, \xi, \boldsymbol{c}, \Xi, \omega_{s,p}, T_p, m_p, t) \, \mathrm{d}\boldsymbol{c} \, \mathrm{d}\Xi \, \mathrm{d}\omega_{s,p} \, \mathrm{d}T_p \, \mathrm{d}m_p \end{aligned} \tag{7}$$

Average fluid properties can be found by inserting for ψ_p in Eq. (7) as shown by e.g. Laurent and Massot (2001) and Lathouwers and Bellan (2000). The average mass for the bubbles at position $\boldsymbol{r}$ with size ξ at time t is found as:

$$\begin{aligned} m(\boldsymbol{r}, \xi, t) &= \langle m_p \rangle \\ &= \frac{1}{f_d(\boldsymbol{r}, \xi, t)} \int_{-\infty}^{+\infty} m_p m_p p(\boldsymbol{r}, \xi, \boldsymbol{c}, \Xi, \omega_{s,p}, T_p, m_p, t) \, \mathrm{d}\boldsymbol{c} \, \mathrm{d}\Xi \, \mathrm{d}\omega_{s,p} \, \mathrm{d}T_p \, \mathrm{d}m_p \end{aligned} \tag{8}$$

Similarly to Lathouwers and Bellan (2000) we adapt the relation:

$$f_d(\boldsymbol{r}, \xi, t) = f(\boldsymbol{r}, \xi, t) m(\boldsymbol{r}, \xi, t) \tag{9}$$

where $f(\boldsymbol{r}, \xi, t)$ is the average number density (Eq. (3)) and $m(\boldsymbol{r}, \xi, t)$ is the average mass (Eq. (8)). The mass average fluid velocity $\boldsymbol{v_r}(\boldsymbol{r}, \xi, t)$ is found by inserting for the microscopical velocity velocity $\boldsymbol{c}$ in Eq. (7):

$$\boldsymbol{v_r}(\boldsymbol{r}, \xi, t) = \frac{1}{f_d(\boldsymbol{r}, \xi, t)} \int_{-\infty}^{+\infty} \boldsymbol{c} m_p p(\boldsymbol{r}, \xi, \boldsymbol{c}, \Xi, \omega_{s,p}, T_p, m_p, t) \, \mathrm{d}\boldsymbol{c} \, \mathrm{d}\Xi \, \mathrm{d}\omega_{s,p} \, \mathrm{d}T_p \, \mathrm{d}m_p \tag{10}$$

The deviation from the average fluid velocity is denoted the peculiar velocity

$$\boldsymbol{C}(\boldsymbol{r}, \xi, \boldsymbol{c}, \Xi, \omega_{s,p}, T_p, m_p, t) = \boldsymbol{c} - \boldsymbol{v_r}(\boldsymbol{r}, \xi, t) \tag{11}$$

The moment (Eq. (7)) of the peculiar velocity is zero (e.g. Solsvik and Jakobsen (2016)). The mass averaged growth velocity, i.e. convection in property space, is found by inserting for $\psi_p = \Xi$ in Eq. (7):

$$v_\xi(\boldsymbol{r}, \xi, t) = \frac{1}{f_d(\boldsymbol{r}, \xi, t)} \int_{-\infty}^{+\infty} \Xi m_p p(\boldsymbol{r}, \xi, \boldsymbol{c}, \Xi, \omega_{s,p}, T_p, m_p, t) \, \mathrm{d}\boldsymbol{c} \, \mathrm{d}\Xi \, \mathrm{d}\omega_{s,p} \, \mathrm{d}T_p \, \mathrm{d}m_p \tag{12}$$

The deviation from the average bubble growth velocity is denoted the peculiar growth velocity:

$$C_\xi(\boldsymbol{r}, \xi, \boldsymbol{c}, \Xi, \omega_{s,p}, T_p, m_p, t) = \Xi - v_\xi(\boldsymbol{r}, \xi, t) \tag{13}$$

169 Following an argument similar to the physical velocity the average of the peculiar
170 growth velocity is zero. Similarly we have for the mass averaged weight fraction:

$$\begin{aligned}&\omega_s(\boldsymbol{r},\xi,t)\\&=\frac{1}{f_d(\boldsymbol{r},\xi,t)}\int_{-\infty}^{+\infty}\omega_{s,p}m_p p(\boldsymbol{r},\xi,\boldsymbol{c},\Xi,\omega_{s,p},T_p,m_p,t)\,\mathrm{d}\boldsymbol{c}\,\mathrm{d}\Xi\,\mathrm{d}\omega_{s,p}\,\mathrm{d}T_p\,\mathrm{d}m_p\end{aligned}\tag{14}$$

171 The mass averaged enthalpy is given as:

$$h(\boldsymbol{r},\xi,t)=\frac{1}{f_d(\boldsymbol{r},\xi,t)}\int_{-\infty}^{+\infty}h_p m_p p(\boldsymbol{r},\xi,\boldsymbol{c},\Xi,\omega_{s,p},T_p,m_p,t)\,\mathrm{d}\boldsymbol{c}\,\mathrm{d}\Xi\,\mathrm{d}\omega_{s,p}\,\mathrm{d}T_p\,\mathrm{d}m_p\tag{15}$$

172 The fluctuating weight fraction and enthalpy are defined as the difference between
173 the microscopical (particle) quantity and the average quantity:

$$\omega_s'(\boldsymbol{r},\xi,\boldsymbol{c},\Xi,\omega_{s,p},T_p,m_p,t)=\omega_{s,p}-\omega_s(\boldsymbol{r},\xi,t)\tag{16}$$

174

$$h'(\boldsymbol{r},\xi,\boldsymbol{c},\Xi,\omega_{s,p},T_p,m_p,t)=h_p-h(\boldsymbol{r},\xi,t)\tag{17}$$

175 for which the averages are zero. The pressure tensor and the heat flux are given
176 by:

$$\begin{aligned}\boldsymbol{P}_{\boldsymbol{r}}(\boldsymbol{r},\xi,t)&=\int_{-\infty}^{+\infty}m_p\boldsymbol{C}\boldsymbol{C}p(\boldsymbol{r},\xi,\boldsymbol{c},\Xi,\omega_{s,p},T_p,m_p,t)\,\mathrm{d}\boldsymbol{c}\,\mathrm{d}\Xi\,\mathrm{d}\omega_{s,p}\,\mathrm{d}T_p\,\mathrm{d}m_p\\&=f_d\langle\boldsymbol{C}\boldsymbol{C}\rangle\end{aligned}\tag{18}$$

177

$$\begin{aligned}\boldsymbol{q_r}(\boldsymbol{r},\xi,t) &= \int_{-\infty}^{+\infty} m_p \boldsymbol{C} h' p(\boldsymbol{r},\xi,\boldsymbol{c},\Xi,\omega_{s,p},T_p,m_p,t)\ \mathrm{d}\boldsymbol{c}\ \mathrm{d}\Xi\ \mathrm{d}\omega_{s,p}\ \mathrm{d}T_p\ \mathrm{d}m_p \\ &= f_d\langle \boldsymbol{C} h'\rangle\end{aligned} \tag{19}$$

178 by use of Eq. (5) and Eq. (6). Similarly, we define a space-property pressure vector
179 and a space-property kinetic energy flux:

$$\boldsymbol{p_\xi} = \int_{-\infty}^{+\infty} m_p C_\xi \boldsymbol{C} p(\boldsymbol{r},\xi,\boldsymbol{c},\Xi,\omega_{s,p},T_p,m_p,t)\ \mathrm{d}\boldsymbol{c}\ \mathrm{d}\Xi\ \mathrm{d}\omega_{s,p}\ \mathrm{d}T_p\ \mathrm{d}m_p = f_d\langle C_\xi \boldsymbol{C}\rangle \tag{20}$$

180

$$q_\xi = \int_{-\infty}^{+\infty} m_p C_\xi h' p(\boldsymbol{r},\xi,\boldsymbol{c},\Xi,\omega_{s,p},T_p,m_p,t)\ \mathrm{d}\boldsymbol{c}\ \mathrm{d}\Xi\ \mathrm{d}\omega_{s,p}\ \mathrm{d}T_p\ \mathrm{d}m_p = f_d\langle C_\xi h'\rangle \tag{21}$$

181 The pressure tensor, space-property pressure vector, heat flux and space-property
182 heat flux are discussed in section 3.

183 *2.2. The Boltzmann Equation*

184 A Boltzmann-like equation can be formulated as a continuity statement in the phase
185 space for the particle (Andresen, 1990; Lathouwers and Bellan, 2000; Laurent and
186 Massot, 2001; Nayak et al., 2011):

$$\begin{aligned}&\frac{\partial p}{\partial t} + \boldsymbol{c}\cdot\frac{\partial p}{\partial \boldsymbol{r}} + \dot{\boldsymbol{c}}\cdot\frac{\partial p}{\partial \boldsymbol{c}} + \Xi\frac{\partial p}{\partial \xi} + \dot{\Xi}\frac{\partial p}{\partial \Xi} + \dot{T}_p\frac{\partial p}{\partial T_p} + \sum_c \dot{\omega}_{c,p}\frac{\partial p}{\partial \omega_{c,p}} + \dot{m}_p\frac{\partial p}{\partial m_p} \\ &= \left(\frac{\partial p}{\partial t}\right)_{\text{collision}} + S\end{aligned} \tag{22}$$

187 where the generalized coordinates $\boldsymbol{r}$, ξ, T_p, $\omega_{c,p}$, m_p and generalized velocities $\boldsymbol{c}$,
188 Ξ, $\dot{T}_p$, $\dot{\omega}_{c,p}$, $\dot{m}_p$ are assumed independent of each other, but dependent on time.
189 The Boltzmann-like equation describes the evolution of the microscopical number

density p in the phase space. We denote it Boltzmann-*like* to distinguish it from the conventional Boltzmann equation formulated in the space $[\boldsymbol{r}, \boldsymbol{c}]$ (see e.g. Jakobsen (2014)). The terms on the right hand side $\left(\frac{\partial p}{\partial t}\right)_{\text{collision}}$ and S are source terms for events due to collisions and for events not related to collisions respectively.

Solving Eq. (22) for all bubbles in a reactor is not (yet) computationally feasible for industrial applications. Instead, we can form a generalized moment equation by multiplying with a microscopical quantity ψ_p and integrate over the velocity space $[\boldsymbol{c}, \Xi]$, temperature and weight fractions (Andresen, 1990; Lathouwers and Bellan, 2000). By inserting for different quantities for ψ_p, we can obtain equations of change for the dispersed phase properties such as mass density, weight fractions, momentum and enthalpy/temperature.

As our derivation of the moment equation differs slightly from the literature (Andresen, 1990; Lathouwers and Bellan, 2000; Nayak et al., 2011) it is written out in Appendix A. The result is Eq. (23) which is a moment equation for the generalized quantity ψ_p:

$$
\begin{aligned}
&\frac{\partial}{\partial t}(f_d\langle\psi_p\rangle) + \frac{\partial}{\partial \boldsymbol{r}} \cdot (f_d\langle\psi_p \boldsymbol{c}\rangle) + \frac{\partial}{\partial \xi}(f_d\langle\Xi\psi_p\rangle) = \\
&f_d\left[\langle\frac{\partial \psi_p}{\partial t}\rangle + \langle \boldsymbol{c} \cdot \frac{\partial \psi_p}{\partial \boldsymbol{r}}\rangle + \langle \dot{\boldsymbol{c}} \cdot \frac{\partial \psi_p}{\partial \boldsymbol{c}}\rangle + \langle \Xi \frac{\partial \psi_p}{\partial \xi}\rangle + \langle \dot{\Xi}\frac{\partial \psi_p}{\partial \Xi}\rangle\right] \\
&+ f_d\left[\langle \dot{T}_p \frac{\partial \psi_p}{\partial T_p}\rangle + \sum_c \langle \dot{\omega}_{c,p}\frac{\partial \psi_p}{\partial \omega_{c,p}}\rangle + \langle \dot{m}_p\left(\frac{\partial \psi_p}{\partial m_p} + \frac{1}{m_p}\right)\rangle\right] \\
&+ \langle S_{\psi_p}\rangle
\end{aligned}
\tag{23}
$$

where $\langle\rangle$ denotes a mass average (Eq. (7)). Eq. (23) differs from Andresen (1990)

and Lathouwers and Bellan (2000) with its convective term in the particle size ξ on the left hand side and two particle size related terms on the right hand side. It differs from the work of Nayak et al. (2011) by including temperature and weight fraction. The source term $\langle S_{\psi_p} \rangle$ is a combined source term consisting of both source terms due to particle collisions and source terms not related to particle collisions.

Slightly different interpretations of ψ_p are found in the literature. Lathouwers and Bellan (2000) defined ψ_p as a particle property which was independent of time. Patruno (2010) inserted for $\psi_p = \rho_G V(\xi)$ where the density was assumed constant. Andresen (1990) defined ψ_p as a generic weighting function $g = g(\boldsymbol{r}, s, \boldsymbol{c}, T_p, t)$ where s is size. In this study ψ_p denotes a microscopic quantity, i.e. a property at the particle level, which is assumed independent of time. The first term on the right hand side in Eq. (23) then disappears.

2.3. Derivation of the equations of change

The equations of change for species mass, total mass, momentum and enthalpy/temperature can be derived from Eq. (23) by inserting for the appropriate microscopic quantities. The derivation similar to the work by Lathouwers and Bellan (2000) for solid particles, but extended to include particle size to describe bubbly flow. The derivation is outlined in Appendix B. The equation of change for total mass is given as:

$$\frac{\partial f_d}{\partial t} + \frac{\partial}{\partial \boldsymbol{r}} \cdot (f_d \boldsymbol{v}_{\boldsymbol{r}}) + \frac{\partial}{\partial \xi}(f_d v_\xi) = f_d \langle \frac{\mathrm{d}m_p}{\mathrm{d}t} \left(\frac{1}{m_p} \right) \rangle + \langle S_1 \rangle \tag{24}$$

The equation of change for species mass is given as:

$$\begin{aligned}&\frac{\partial(f_d\omega_s)}{\partial t}+\frac{\partial}{\partial \boldsymbol{r}}\cdot(f_d\boldsymbol{v_r}\omega_s)+\frac{\partial}{\partial \xi}(f_d v_\xi \omega_s)\\&=-\frac{\partial}{\partial \boldsymbol{r}}\cdot(f_d\langle \boldsymbol{C}\omega_s'\rangle)-\frac{\partial}{\partial \xi}(f_d\langle C_\xi\omega_s'\rangle)+f_d\langle\frac{1}{m_p}\frac{dm_{s,p}}{\mathrm{d}t}\rangle+\langle S_{\omega_{s,p}}\rangle\end{aligned} \tag{25}$$

The equation of change for momentum is given as:

$$\begin{aligned}&\frac{\partial(f_d\boldsymbol{v_r})}{\partial t}+\frac{\partial}{\partial \boldsymbol{r}}\cdot(f_d\boldsymbol{v_r}\boldsymbol{v_r})+\frac{\partial}{\partial \xi}(f_d v_\xi \boldsymbol{v_r})\\&=-\frac{\partial}{\partial \boldsymbol{r}}\boldsymbol{P_r}-\frac{\partial}{\partial \xi}\boldsymbol{p_\xi}+f_d\boldsymbol{F_r}+f_d\langle\frac{\mathrm{d}m_p}{\mathrm{d}t}\frac{\boldsymbol{c}}{m_p}\rangle+\langle S_{\boldsymbol{c}}\rangle\end{aligned} \tag{26}$$

Finally, the equation of change for enthalpy in terms of temperature is given as:

$$\begin{aligned}&f_dC_p\frac{\partial T}{\partial t}+f_dC_p\boldsymbol{v_r}\frac{\partial T}{\partial \boldsymbol{r}}+f_dC_pv_\xi\frac{\partial T}{\partial \xi}=-\frac{\partial}{\partial \boldsymbol{r}}\cdot\boldsymbol{q_r}-\frac{\partial}{\partial \xi}q_\xi-\sum_s\left(\frac{\partial h}{\partial \omega_s}\right)_{T,p}\frac{D_a\omega_s}{D_at}\\&-f_d\langle\frac{Q_{cd,p}}{m_p}\rangle-f_d\langle\frac{1}{m_p}\sum_s\frac{\mathrm{d}m_{p,s}}{\mathrm{d}t}(h_v-h_{p,s})\rangle+f_d\langle\frac{\mathrm{d}m_p}{\mathrm{d}t}\frac{h_p}{m_p}\rangle-f_dh\langle\frac{\mathrm{d}m_p}{\mathrm{d}t}\frac{1}{m_p}\rangle\\&+\langle S_{h_p}\rangle-h\langle S_1\rangle\end{aligned} \tag{27}$$

The equations of change contain a transient term and two convective terms; one due to convective transport in spatial space and one due to convection in property (size) space. On the right hand side the equations (except Eq. (24)) contain dispersion terms for spatial and property space, interphase exchange terms and source terms. A further discussion of the terms along with suggested closures is given in Section 3.

2.4. Comparison with existing models

The equations for total mass, species mass, momentum and enthalpy (Eq.s (24), (25), (26) and (27)) are similar to those by Lathouwers and Bellan (2001) except the terms that account for the bubble size. The equations of change for mass and momentum (Eq. (24) and (26)) are identical to previous work by Nayak et al. (2011) except the interfacial mass transfer term.

Eq. (24) and Eq. (26) differ from the inhomogeneous MUSIG model (Krepper et al., 2008) on several points. Firstly the proposed model in this work requires one continuity equation (which is the PBE; Eq. (24)) to describe the evolution of the mass density of particles. In the MUSIG models one PBE for each particle size group i is required. Similarly, in the proposed model in this work one momentum equation is sufficient to describe the dispersed phase velocity field for the entire bubble population. In contrast, the inhomogeneous MUSIG model has one momentum equation and one continuity equation for each velocity group j. Finally, temperature and species mass equations for the inhomogeneous MUSIG model are not found in the literature as only isothermal, non-reactive flow studies have been reported so far.

The bubble size distribution, gas composition, gas temperature and the bubble velocity in the heterogeneous flow regime may be more accurately represented by a continuous function of bubble size than by a set of discrete size sections. If the number of size and velocity sections in the MUSIG model were increased sufficiently to approximate continuous functions, the computational time for the MUSIG models would increase accordingly. This must be taken into account when comparing

computational time of the proposed model to the MUSIG models.

2.5. Continuous phase equations

The dispersed phase equations were given in the previous section. To arrive at a multifluid-PBE model equations for the continuous phase, in this case the liquid phase, are also required. These can be found e.g. in Jakobsen (2014) in the form of local instantaneous equations of change for total mass, species mass, momentum and enthalpy (temperature).

3. Closures

To solve the multifluid-PBE model suitable closures must be derived for the dispersion terms, exchange terms, source terms and the growth velocity. These will be discussed in the sequel.

3.1. Diffusive terms

Diffusive terms arise from the average of fluctuation products derived in Eq.s (B.5), (B.6), (B.13), (B.14), (B.19) and (B.20). They are in the following referred to as dispersion terms (equation of change for weight fractions), stress tensor (equation of change for momentum) and heat conduction terms (equation of change for temperature).

In the proposed model the diffusive terms do not appear in the PBE (Eq. (24)). In the literature the inclusion of diffusive terms in the PBE has been discussed by Sporleder

et al. (2012). They found no physical diffusive mechanisms for laminar flow, but for turbulent flow they occurred if Reynolds averaging of the equation was applied. Some models added diffusive terms to the PBE to account for an observed phenomenon, for example Randolph and Larson (1988) who accounted for the random fluctuation in growth rate and axial flow by adding the terms $\frac{\partial}{\partial \xi}\left(D_\xi \frac{\partial f}{\partial \xi}\right)$ and $\nabla_{\boldsymbol{r}} \cdot (\boldsymbol{D_r} \nabla_{\boldsymbol{r}} f)$ to account for diffusivity in the property and spatial space, respectively.

3.1.1. Dispersion terms

In the current modeling framework the dispersion terms in physical space occur as the average of the product of the peculiar velocity and the fluctuations in the weight fraction. The peculiar velocity $\boldsymbol{C}$ describes the fluctuating bubble velocity and is not the peculiar species velocity, as its parallel $\boldsymbol{C}_s$ in kinetic gas theory (Hirschfelder et al., 1954; Solsvik and Jakobsen, 2016). The fluctuation term $\frac{\partial}{\partial \boldsymbol{r}} \cdot (f_d \langle \boldsymbol{C} \omega_s' \rangle)$ may be interpreted as a bubble dispersion term due to fluctuations in bubble velocity and written as a mass flux Chao (2012); Lindborg (2008): $f_d \langle \boldsymbol{C} \omega_s' \rangle = \boldsymbol{j_{r,s}}$. This flux may be parameterized by a Fickian closure.

The dispersion term in the property space $\frac{\partial}{\partial \xi}(f_d \langle C_\xi \omega_s' \rangle)$ can be interpreted as the fluctuations in growth velocity due to fluctuations in the composition.

3.1.2. The bubble pressure tensor and the bubble space-property pressure vector

In KTGF the pressure tensor is a well-known quantity. It can be modeled as a linear sum of e.g. kinetic, collisional and frictional contributions (e.g. Lindborg

(2008)):

$$\boldsymbol{P} = \boldsymbol{P}^k + \boldsymbol{P}^c + \boldsymbol{P}^f \tag{28}$$

In disperse bubbly flows the bubble pressure tensor is commonly neglected. However, analogous to KTGF it can be modeled as a linear sum of kinetic, collisional and hydrodynamic contributions (Spelt and Sangani, 1998). In addition, Biesheuvel and van Wijngaarden (1984) considered a contribution due to the change in volume of the bubbles due to mass transfer. This gives for the bubble pressure tensor:

$$\boldsymbol{P}_b = \boldsymbol{P}_b^k + \boldsymbol{P}_b^c + \boldsymbol{P}_b^h + \boldsymbol{P}_b^m \tag{29}$$

Only the kinetic contribution appears in the presented derivation of Eq. (26). The collisional contribution is neglected here as we assume elastic collisions. The hydrodynamic contribution is also neglected. The mass transfer contribution is discussed below.

The kinetic contributions are analogous in granular and bubbly flow. Both are derived from the average of the product of the fluctuating peculiar velocities, as shown for disperse bubbly flows in Eq. (18). The physical interpretation of the kinetic contribution is a momentum production by the fluctuating motion of the bubbles. The kinetic pressure tensor (and the other tensors in Eq. (29)) can be decomposed into a pressure and a deviatoric stress:

$$\boldsymbol{P}_b^k = p_b^k \boldsymbol{I} + \boldsymbol{\sigma} \tag{30}$$

where p_b^k is the bubble pressure and $\boldsymbol{\sigma}$ is a deviatoric stress term.

Several parameterizations are found for the bubble pressure (Monahan, 2007); as a linear combination of the kinetic, collisional and hydrodynamic effects analogous to KTGF (e.g Spelt and Sangani (1998)), postulated models (Biesheuvel and Gorissen, 1990; Sankaranarayanan and Sundaresan, 2002) or models based on ensemble averaging (Biesheuvel and van Wijngaarden, 1984). It should be noted that none of these are functions of bubble size, but the parameterization by Biesheuvel and van Wijngaarden (1984) does include mass transfer. Monahan (2007) applied the bubble pressure model by Biesheuvel and Gorissen (1990), similar to that of Sankaranarayanan and Sundaresan (2002):

$$p_g = \rho_L C_{BP} \alpha_g (v_G - v_L)^2 H(\alpha) \tag{31}$$

where C_{BP} is a proportionality constant and $H(\alpha)$ (Batchelor, 1988) is a dimensionless function which adjusts the magnitude of the value of the velocity fluctuation $(v_G - v_L)^2$. In the limiting cases of zero gas fraction $\alpha = 0$ and the case for which the particles are packed closely as dense as possible $\alpha = \alpha_{dp}$ the particles are isolated or locked, respectively, and $H(\alpha)$ is zero.

The collisional contribution in Eq. (29) contributes to a spatial spreading out of the particles. This is a similar mathematical effect as of that described by the turbulent dispersion force in poly-disperse flows, which contributes to the spreading of the bubbles out from the pipe center (Lucas et al., 2007) and has been parameterized

as:

$$\boldsymbol{f}_{TD} = \frac{3C_D v_{t,l}}{4\xi Pr}\rho_L(\boldsymbol{v}_G - \boldsymbol{v}_L)\nabla\alpha \tag{32}$$

The physical phenomena represented by the collisional contribution to the particle pressure are considered more realistic than the turbulent dispersion force since the latter appears as a turbulent flux parameterization using a particular ensemble averaging procedure.

The deviatoric stress term $\boldsymbol{\sigma}$ may be parameterized as a viscous stress using Newton's viscous stress tensor:

$$\boldsymbol{\sigma} = -\mu\left[\nabla\boldsymbol{v} + (\nabla\boldsymbol{v})^T\right] + (\frac{2}{3}\mu - \mu_B)(\nabla\cdot\boldsymbol{v})\boldsymbol{e} \tag{33}$$

where μ is the granular or bubble viscosity and μ_B is the bulk viscosity. In practical terms $\boldsymbol{\sigma}$ is a velocity-smoothing term on the bubble scale.

The bubble space-property pressure vector p_ξ may be interpreted as the stress produced due to the diameter (volume) change of the bubbles. It may be decomposed in the same way as the spatial pressure:

$$\boldsymbol{p}_\xi = p_{g,\xi}\boldsymbol{e} + \boldsymbol{\sigma}_\xi \tag{34}$$

where $\boldsymbol{e}$ is the unit vector and $\boldsymbol{\sigma}_\xi$ is a vector. $p_{g,\xi}$ is the contribution by bubble growth to the pressure and $\boldsymbol{\sigma}_\xi$ is the bubble growth contribution to stress. $p_{g,\xi}$ resembles the volume change contribution to the bubble pressure in the interpretation by Biesheuvel and van Wijngaarden (1984).

3.1.3. The heat flux in physical and property space

The average of the product of the peculiar velocity and enthalpy fluctuations in physical space is interpreted as the heat flux $\boldsymbol{q_r}$. This covariance terms may be parameterized by a conduction flux similar to Fourier's law (Chao, 2012; Lindborg, 2008):

$$f_d\langle \boldsymbol{C}h'\rangle = -k\nabla T \tag{35}$$

The space-property heat flux q_ξ is interpreted as the heat generated by the covariance between the particular velocity and the fluctuation in the growth velocity for the bubbles. No parameterizations of this term are known to the authors.

The discussion above considers molecular temperature. A related temperature is the particle temperature, in KTGF well known as granular temperature. An analogous temperature for the bubble phase is called the bubble phase temperature, discussed along with its suggested equation of change in Spelt and Sangani (1998), but not further discussed here.

3.2. Growth velocity

The average growth velocity v_ξ describes the average time rate of change for the bubble diameter. It is an average for all bubbles at location $\boldsymbol{r}$ and of size ξ at time t. This means that all bubbles at the same location, size and time will have equal growth rates. Morel (2015) used the material derivative in the physical space to express the growth rate of a bubble. He utilized an expression for the growth rate

based on a mass balance for a single bubble:

$$\frac{\mathrm{D}m}{\mathrm{D}t} = \frac{\mathrm{D}\rho_G V}{\mathrm{D}t} = \rho_G \frac{\mathrm{D}V}{\mathrm{D}t} + V\frac{\mathrm{D}\rho_G}{\mathrm{D}t} = -\gamma_p \rightarrow \frac{\mathrm{D}V}{\mathrm{D}t} = -\frac{V}{\rho_G}\frac{\mathrm{D}\rho_G}{\mathrm{D}t} - \frac{\gamma_p}{\rho_G} \tag{36}$$

In terms of diameter, $\frac{DV}{\mathrm{D}t} = \frac{\pi}{2}\xi^2\frac{D\xi}{\mathrm{D}t}$:

$$\frac{\mathrm{D}\xi}{\mathrm{D}t} = -\frac{\xi}{3\rho_G}\frac{\mathrm{D}\rho_G}{\mathrm{D}t} - \frac{\gamma_p}{\frac{\pi}{2}\xi^2\rho_G} = -\frac{\xi}{3\rho_G}\left[\frac{\partial \rho_G}{\partial t} + \boldsymbol{v_r}\cdot\nabla_r\rho_G\right] - \frac{\gamma_p}{\frac{\pi}{2}\xi^2\rho_G} \equiv v_\xi \tag{37}$$

A similar expression is applied in the work of Millies and Mewes (1996), Mewes and Wiemann (2007) and Buffo et al. (2013).

In the current model the interfacial mass transfer flux is included in a separate mass transfer source term (Section 3.3.1). The growth term thus contains only the gas expansion term due to external pressure changes.

The separate source term for mass transfer appears directly in the equation through the averaging procedure using a mass density function. In the book of Randolph and Larson (1988) a similar term is included in the PBE for employing a *mass* density function for the population of crystals (but not in their PBE for *number* density functions).

The phenomena contributing to the growth velocity are temperature change, pressure change and change in number of moles of gas in the bubble. Formulating a PBE for the number density function it is common practice to include the mass transfer flux through the growth term. The current model actually allows for the mass transfer flux to be included in both terms which is not considered a consistent approach.

3.3. Exchange terms

3.3.1. Mass transfer terms

The interfacial mass transfer terms appear on the right hand side of all equations of change in the proposed multifluid-PBE model (Eq.s (24), (25), (26) and (27)). We here consider bubbles in a liquid and thus gas-liquid mass transfer. In gas-liquid mass transfer the transport through the liquid side film is commonly the rate limiting step because the diffusivity is smaller in the liquid film than in the gas phase. The mass transfer term for species s in a single bubble can be parameterized as:

$$\frac{\mathrm{d}m_{p,s}}{\mathrm{d}t} = \dot{m_{p,s}} A = A\rho_L k_{L,s}(\omega^*_{L,s} - \omega_{L,s}) \tag{38}$$

where $\dot{m_{p,s}}$ is the rate of mass entering or leaving the bubble, A is the surface area of the bubble, $k_{L,s}$ the mass transfer coefficient, ρ_L the liquid density and $\omega^*_{L,s}$, $\omega_{L,s}$ the weight fractions of species s at the gas-liquid interface and in the liquid bulk, respectively. By multiplying Eq. (38) with $\frac{f_d}{\rho_G V}$ we get the mass transfer of species s for all bubbles at location $\boldsymbol{r}$ with size ξ at time t, which is the term required in Eq. (25). We may thus write:

$$\begin{aligned} f_d(\boldsymbol{r},\xi,t)\langle\frac{1}{m_p}\frac{\mathrm{d}m_{s,p}}{\mathrm{d}t}\rangle &\approx f_d(\boldsymbol{r},\xi,t)\gamma_s(\boldsymbol{r},\xi,t) \\ &\approx \frac{f_d(\boldsymbol{r},\xi,t)}{\rho_G(\boldsymbol{r},\xi,t)V(\xi)} A(\xi)\rho_L k_{L,s}(\boldsymbol{r},\xi)(\omega^*_{L,s}(\boldsymbol{r},\xi,t) - \omega_{L,s}(\boldsymbol{r},\xi,t)) \end{aligned} \tag{39}$$

The total mass transfer is found by summing over all species s:

$$f_d(\boldsymbol{r},\xi,t)\langle\frac{1}{m_p}\frac{\mathrm{d}m_p}{\mathrm{d}t}\rangle \approx f_d(\boldsymbol{r},\xi,t)\gamma(\boldsymbol{r},\xi,t) = \sum_s f_d(\boldsymbol{r},\xi,t)\langle\frac{1}{m_p}\frac{\mathrm{d}m_{s,p}}{\mathrm{d}t}\rangle$$
$$\approx \sum_s \frac{f_d(\boldsymbol{r},\xi,t)}{\rho_G(\boldsymbol{r},\xi,t)V(\xi)}A(\xi)\rho_L k_{L,s}(\boldsymbol{r},\xi)(\omega^*_{L,s}(\boldsymbol{r},\xi,t)-\omega_{L,s}(\boldsymbol{r},\xi,t)) \tag{40}$$

3.3.2. Momentum transfer terms

The momentum transfer terms are given in Eq. (B.15). The drag force is parameterized as shown by Nayak et al. (2011):

$$\boldsymbol{f}^{G-L}_{\mathrm{drag}}(\boldsymbol{r},\xi,t) = \frac{3}{4}\rho_L\frac{C_{D,G}}{\xi}\frac{f_d(\boldsymbol{r},\xi,t)}{\rho_G(\boldsymbol{r},\xi,t)}|\boldsymbol{v}_L(\boldsymbol{r},t)-\boldsymbol{v}_G(\boldsymbol{r},\xi,t)|(\boldsymbol{v}_L(\boldsymbol{r},t)-\boldsymbol{v}_G(\boldsymbol{r},\xi,t)) \tag{41}$$

where $C_{D,G}$ is the drag coefficient and $\boldsymbol{v}_L(\boldsymbol{r},t)-\boldsymbol{v}_G(\boldsymbol{r},\xi,t)$ is the velocity difference between the dispersed and the continuous phase. The lift force may be parameterized as (Krepper et al., 2008):

$$\boldsymbol{f}_{\mathrm{lift}} = -C_L\rho_L\alpha(\boldsymbol{v}_G-\boldsymbol{v}_L)\times(\nabla\times\boldsymbol{v}_G) \tag{42}$$

where C_L is the lift coefficient. Expressing the lift force in terms of bubble size we may suggest:

$$\boldsymbol{f}_{\mathrm{lift}} = -C_L\rho_L\frac{f_d(\boldsymbol{r},\xi,t)}{\rho_G(\boldsymbol{r},\xi,t)V(\xi)}\left[\boldsymbol{v}_G(\boldsymbol{r},\xi,t)-\boldsymbol{v}_L(\boldsymbol{r},t)\right]\times(\nabla\times\boldsymbol{v}_G(\boldsymbol{r},\xi,t)) \tag{43}$$

The virtual mass force accounts for the acceleration of the fluid caused by the rising bubbles as they displace the liquid on their way. For the virtual mass force we may write (Jakobsen, 2014):

$$\boldsymbol{f}_{\mathrm{vm}} = \rho_L C_{VM} \frac{f_d(\boldsymbol{r},\xi,t)}{\rho_G(\boldsymbol{r},\xi,t)} \left(\frac{\mathrm{D}\boldsymbol{v}_L(\boldsymbol{r},t)}{\mathrm{D}t} - \frac{\mathrm{d}\boldsymbol{v}_G((\boldsymbol{r},\xi,t))}{\mathrm{d}t} \right) \tag{44}$$

where C_{VM} is the virtual mass coefficient and $\frac{\mathrm{D}}{\mathrm{D}t}$ is the substantial derivative in physical space.

3.3.3. Heat transfer terms

The heat transfer term in the dispersed phase is given as $f_d\langle\frac{Q_{cd,p}}{m_p}\rangle$ and is parameterized in the following for gas bubbles in a liquid. The heat exchange between gas bubbles and the liquid is modeled as the product between the available surface area and the driving force, similar to the mass transfer and drag terms. The available surface area for heat transfer is the same as for mass transfer. The driving force is the temperature difference between the gas and the liquid and we assume uniform temperature for all bubbles who share the same size and the same location. Along with the heat exchange coefficient h_{G-L} this gives the expression for the gas-liquid heat exchange as a function of bubble size, spatial space and time:

$$\begin{aligned} f_d\langle\frac{Q_{cd,p}}{m_p}\rangle &\approx f_d(\boldsymbol{r},\xi,t) q_c(\boldsymbol{r},\xi,t) \\ &= \frac{f_d(\boldsymbol{r},\xi,t) A(\xi) h_{G-L}(\boldsymbol{r},\xi,t)}{\rho_G(\boldsymbol{r},\xi,t) V(\boldsymbol{r},\xi,t)} (T_G(\boldsymbol{r},\xi,t) - T_L(\boldsymbol{r},t)) \end{aligned} \tag{45}$$

3.4. Source terms

The source term $\langle S_{\psi_p} \rangle$ includes both the collision term $\langle \psi_p \frac{\partial p}{\partial t}_{\text{collisions}} \rangle$ and a generalized source term $\langle \psi_p S \rangle$ independent of collisions (Nayak et al., 2011).

The collision term $\langle \psi_p \frac{\partial p}{\partial t}_{\text{collisions}} \rangle$ is in general zero for a conserved quantity when assuming elastic collisions. Under this assumption the mass, species mass, momentum and total energy are all conserved quantities in the event of a collision and we can write $\langle S_{\psi_p} \rangle = \langle \psi_p S \rangle$

The generalized source term $\langle S_{\psi_p} \rangle$ is here assumed to include events such as breakage and coalescence. Breakage and coalescence are important phenomena for industrial bubble column reactors operated in the heterogeneous regime. The models for breakage and coalescence phenomena are generally built on mechanical principles and introduced in the equations of change instead of being derived from the kinetic theory of gases. Many different closure models are available (see e.g. Solsvik et al. (2013) for a review on breakage models, Liao and Lucas (2010) for coalescence models).

The source term $\langle S_{\psi_p} \rangle$ appears in all equations of change for the dispersed phase in the multifluid-PBE model proposed, but only the parameterization for the PBE (Eq. (24)) is known to the authors. A source term related to coalescence and breakage is mentioned in the work by Krepper et al. (2008). For a number density function with diameter as inner coordinate the PBE with source terms for breakage and

coalescence can be given as (Nayak et al., 2011; Zhu, 2009):

$$\begin{aligned}
&\frac{\partial f(\boldsymbol{r},\xi,t)}{\partial t}+\frac{\partial}{\partial \boldsymbol{r}}\cdot(f(\boldsymbol{r},\xi,t)\boldsymbol{v_r}(\boldsymbol{r},\xi,t))+\frac{\partial}{\partial \xi}(f(\boldsymbol{r},\xi,t)v_\xi(\boldsymbol{r},\xi,t))=\\
&-b(\xi)f(\boldsymbol{r},\xi,t)+\int_{\xi}^{\xi_{max}}h_b(\xi,\zeta)b(\zeta)f(\boldsymbol{r},\xi,t)d\zeta\\
&-f(\boldsymbol{r},\xi,t)\int_{\xi_{min}}^{(\xi_{max}^3-\xi^3)^{1/3}}c(\xi,\zeta)f(\boldsymbol{r},\xi,t)d\zeta\\
&+\frac{\xi^2}{2}\int_{\xi_{min}}^{(\xi^3-\xi_{min}^3)^{1/3}}\frac{c([\xi^3-\zeta^3]^{1/3},\zeta)f(\boldsymbol{r},[\xi^3-\zeta^3]^{1/3},t)f(\boldsymbol{r},\zeta,t)}{[\xi^3-\zeta^3]^{2/3}}d\zeta
\end{aligned}\tag{46}$$

Expressing the density function of bubbles in terms of a mass density function $f_d(\boldsymbol{r},\xi,t)=m(\boldsymbol{r},\xi,t)f(\boldsymbol{r},\xi,t)=\rho_G(\boldsymbol{r},\xi,t)V(\xi)f(\boldsymbol{r},\xi,t)$ with the gas density being a function of bubble size gives

$$\begin{aligned}
&S_m(\boldsymbol{r},\xi,t)=-b(\xi)f_d(\boldsymbol{r},\xi,t)\\
&+\rho_G(\boldsymbol{r},\xi,t)V(\xi)\int_{\xi}^{\xi_{max}}h_b(\xi,\zeta)b(\zeta)\frac{f_d(\boldsymbol{r},\zeta,t)}{\rho_G(\boldsymbol{r},\zeta,t)V(\zeta)}d\zeta\\
&-f_d(\boldsymbol{r},\xi,t)\int_{\xi_{min}}^{(\xi_{max}^3-\xi^3)^{1/3}}c(\xi,\zeta)\frac{f_d(\boldsymbol{r},\zeta,t)}{\rho_G(\boldsymbol{r},\zeta,t)V(\zeta)}d\zeta\\
&+\frac{\xi^2\rho_G(\boldsymbol{r},\xi,t)V(\xi)}{2}\times\\
&\int_{\xi_{min}}^{(\xi^3-\xi_{min}^3)^{1/3}}\frac{c([\xi^3-\zeta^3]^{1/3},\zeta)f_d(\boldsymbol{r},[\xi^3-\zeta^3]^{1/3},t)f_d(\boldsymbol{r},\zeta,t)}{[\xi^3-\zeta^3]^{2/3}\rho_G(\boldsymbol{r},\zeta,t)V(\zeta)\rho_G(\boldsymbol{r},[\xi^3-\zeta^3]^{1/3},t)V([\xi^3-\zeta^3]^{1/3})}d\zeta
\end{aligned}\tag{47}$$

which can be applied in Eq. (24).

The event of breakage for a mother bubble into two daughter bubbles is shown in Figure 4. The mass, species mass, momentum and enthalpy of the mother particle will be distributed onto the daughters. The daughters will have the same composition

and temperature as the mother, but not necessarily the same velocity.

Figure 5 shows coalescence of two daughter bubbles with different composition and temperature into a larger mother bubble. The mass, species mass, momentum and enthalpy of the daughters are combined in the mother particle. The mother will have different composition and temperature than the daughters. The momentum of the mother particle will be a sum of the momentum of the daughters.

The source terms due to coalescence and breakage must take care of the redistribution of mass, species mass, momentum and enthalpy in the events of breakage and coalescence. The mass is redistributed according to the source terms in Eq. (47). In the inhomogeneous MUSIG model Krepper et al. (2008) a source term is added to the momentum equation to account for the transfer of momentum between the classes as bubbles move between bubble classes due to coalescence and breakage. A similar term is appropriate in Eq. (26), but on a continuous form. This continuous form is not established yet.

The model formulation proposed in this work has averaged out the microscopical effects of breakage and coalescence, as we have assumed that all bubbles at $\boldsymbol{r}$,ξ,t have the same weight fraction of species s, velocity and temperature. In other words, each single breakage and coalescence event is averaged out, but the mean effects are in principle available through the source term $\langle S_{\psi_p} \rangle$.

The equation of change for species mass must sum to the continuity equation when summing over all species s. This implies for the source terms due to coalescence and

breakage:

$$\sum_s \langle S_{\omega_{p,s}} \rangle = S_m \tag{48}$$

Hence we suggest:

$$\sum_s \langle S_{\omega_{p,s}} \rangle \approx \sum_s \omega_s S_m = S_m \tag{49}$$

For the equation of change for momentum we use a similar approximation, but here assuming that the average of products is equal to the product of averages:

$$\langle S_{\boldsymbol{c}} \rangle \approx \boldsymbol{v_r} S_m \tag{50}$$

Similarly for enthalpy:

$$\langle S_{h_p} \rangle \approx h S_m \tag{51}$$

When continuity is subtracted from the equations of change the source terms equate to zero for the species mass, momentum and temperature equations:

$$\begin{aligned} \langle S_{\omega_{s,p}} \rangle - \omega_s \langle S_1 \rangle &= \langle S_{\omega_{s,p}} \rangle - \omega_s S_m \approx \omega_s S_m - \omega_s S_m = 0 \\ \langle S_{\boldsymbol{c}} \rangle - \boldsymbol{v_r} \langle S_1 \rangle &= \langle S_{\boldsymbol{c}} \rangle - \boldsymbol{v_r} S_m \approx \boldsymbol{v_r} S_m - \boldsymbol{v_r} S_m = 0 \\ \langle S_{h_p} \rangle - h \langle S_1 \rangle &= \langle S_{h_p} \rangle - h S_m \approx h S_m - h S_m = 0 \end{aligned} \tag{52}$$

This means that only the source terms in the PBE remain when subtracting continuity from the equations of change.

4. Model demonstration

To demonstrate the capabilities of the developed model it is applied to the FTS in a SBC. The combined multifluid-PBE model equations are cross-sectional averaged (see e.g. Jakobsen (2014)) and combined with conventional CM equations for the liquid and solid phases. The implemented dispersed phase equations with boundary conditions are given in Appendix C. Operating conditions and reactor dimensions were given in Table 1. Constitutive equations, fluid properties and equations of change for the liquid and solid phases are found in Vik et al. (2015). The model was implemented in MATLAB® and solved using orthogonal collocation.

Bubble size dependent composition, velocity and temperature are shown in Figures 6, 7 and 8. Existing models (e.g. Vik et al. (2015)) show composition and temperature as functions of space. The proposed model shows composition, temperature and velocity as function of space *and bubble size*.

4.1. Bubble size dependent composition

Figure 6 shows the dispersed phase weight fraction of reactant, CO, as function of bubble size ξ and reactor height z (Eq. (C.4)). The bubble size dependency can be seen as the gradient in the ξ direction. As the bubbles move upwards the reactor, CO is transported out of the bubble and into the liquid phase and into the catalyst where it reacts on the active sites. The amount of reactant decreases throughout the reactor, more for the smaller bubbles than for the larger bubbles. The left part of Figure 6 shows the 2D profile, the right part a projected view of the smallest and

largest bubbles. The bold black line shows the average weight fraction of CO as defined in Equation (53). The dashed lines show the vapor-liquid equilibrium weight fraction of CO.

$$\omega_G(z) = \frac{\int_\xi \omega_G(z,\xi) f_d(z,\xi) \mathrm{d}\xi}{\int_\xi f_d(z,\xi) \mathrm{d}\xi} \tag{53}$$

The difference in composition between the smallest and largest bubbles is the distance between the lines with small circles (smallest bubbles) and large circles (largest bubbles) in Figure 6. The larger the distance between the lines, the more different composition in the smallest and largest bubbles. The difference in composition increases along the reactor and slightly decreases towards the end. The maximum absolute value of the difference is 0.13, occurring mid-way in the reactor. The largest percentage difference is at the outlet, of 38%. This means there is a significant difference in concentration between the smallest and largest bubbles.

The mass transfer limitation is the distance between the circled line and the dashed line. The smallest bubbles are closer to equilibrium than the largest bubbles. For the dispersed phase as a whole the mass transfer limitation is visible as the distance between the bold line (the mass average) and the dashed line. The distance between the lines increases toward the middle of the reactor and then decreases. At the outlet the difference between the lines is 0.03 units (25%). This indicates that there is a potential mass transfer limitation for the dispersed phase. Some of the reactant CO, particularly in the larger bubbles, is "stuck" in the gaseous phase and leave the reactor without being transported to the liquid phase where it could have formed products.

4.2. Bubble size dependent velocity

Figure 7 shows the dispersed phase velocity as function of bubble size and axial direction (Eq. (C.6)). The dispersed phase velocity is completely dictated by the drag coefficient. The smallest bubbles follow the liquid due to the boundary condition. The velocity increases with increasing bubble size until 3 mm, where the drag coefficient changes shape. Above this point, the velocity slightly decreases as function of bubble size and then increases for the larger bubbles. The distance between the circled lines, i.e. the difference in velocity between the smallest and largest bubbles, is significant. The mass averaged velocity is closer to the largest bubbles as there are relatively few of the smallest bubbles. The mass averaged velocity (bold line) is about 0.5 m/s. The smallest bubbles have a significantly lower velocity than the largest bubbles, which may contribute to the fact that the smaller bubbles are closer to the equilibrium composition as shown in Figure 6 than the faster-moving larger bubbles.

4.3. Bubble size dependent temperature

Figure 8 shows the dispersed phase temperature as function of bubble size ξ and reactor height z (Eq. (C.8)). The figure shows no visible difference in temperature between the smallest and largest bubbles. In fact, the temperature for the smallest bubbles, the temperature for the largest bubbles, the mass averaged dispersed phase temperature and the slurry temperature are identical. This means that at a given height of the reactor, all bubbles have the same temperature. In other words, the heat exchange is very efficient. This result is expected from the literature, as the

dispersed phase temperature is commonly set to the same as the slurry temperature (see e.g. slurry reactor simulation studies by Lysberg et al. (1989) and Sehabiague et al. (2008)).

4.4. Model potential and comparison to existing models

The capability of the model to predict difference in composition and velocity based on bubble size was demonstrated in Figure 6 and 7. For processes which have strict limitations on the operating criteria the proposed model can give valuable insight. With good models for the mass transfer coefficient, the proposed model can be applied to mass transfer limited processes to study the effect of operating conditions and bubble size to improve conversion. Applications with less efficient heat transfer than the demonstrated FTS conditions will make better use of the model capabilities of predicting bubble size dependent temperature.

To illustrate the model potential the proposed model is compared to an existing model (Vik et al., 2015) in Figure 9. To better demonstrate the bubble size dependency a wider bubble size range was chosen for this comparison. The "large" bubbles suggested by Maretto and Krishna (1999) (20-70 mm) were included by choosing a Sauter mean diameter of 50 mm. The left plots in Figure 9 are the axial profiles of composition, gas density and gas temperature with the existing model (Vik et al., 2015) whilst the right plots in Figure 9 show the axial and bubble size dependent composition, gas density and gas temperature for the proposed model. It is seen that the smaller bubbles, which have a lower velocity (Figure 7) and higher interfacial area per volume have less reactant CO remaining at the reactor outlet. The

largest bubbles have a composition close to their inlet composition. As the FTS converts synthesis gas to hydrocarbons which have a higher molecular weight the change in composition due to mass transfer and subsequent reaction is visible in the gas density plot (Figure 9, middle part).

The proposed model shows how the conversion of reactants into products and the migration of products from the liquid phase and into the gas bubbles is more efficient for smaller bubbles than larger. With a narrow bubble size distribution, most bubbles have a similar composition and the average mass fraction gives sufficient information. However, for a wide bubble size distribution the composition is likely to differ significantly as function of bubble size if mass transfer is the rate limiting step. Large enough bubbles rise fast through the reactor and leave the reactor containing a significant amount of unreacted reactants. In the small enough bubbles all reactant is consumed possibly long before the outlet of the reactor. Thus for wide bubble size distributions the proposed model can suggest an optimized bubble size distribution to improve conversion in the reactor. Coalescence and breakage, which are important phenomena in large industrial reactors, may contribute to a wider bubble size distribution. Thus for large industrial reactors the proposed model can give valuable insights.

The proposed model enables a bubble size dependent mass transfer coefficient, k_L. If k_L is bubble size dependent the shape of the bubble size distribution can affect conversion. Two bubble size distributions with the same gas volume fraction and interfacial area, but with different shape, can in the case of a bubble size dependent k_L result in different conversion. This effect can be accounted for in the proposed

model, but not in conventional models in which neither velocity nor composition are bubble size dependent.

The temperature showed little bubble size dependency for the chosen parameters.

5. Conclusions

In this paper the extension of the continuous multifluid-PBE model to reactive, non-isothermal dispersed flows in order to simulate interfacial mass transfer limited processes was presented. A set of governing equations for the dispersed phase was formulated in terms of a continuous mass density function f_d, with weight fractions and temperature being functions of bubble size. Equations (24), (25), (26) and (27) constitute the model and closures were presented in Section 3.

The capabilities of the model were demonstrated by simulating the FTS operated in a SBC at industrial conditions. Bubble size dependency in both composition and velocity was found; smaller bubbles experienced more efficient transfer of mass and momentum than the larger bubbles. For all bubble sizes the temperature was identical to the slurry temperature due to efficient heat transfer.

The novel model provides a more accurate description of the gas-liquid interfacial area and a more accurate description of the driving force for interfacial mass transfer. The model is thus particularly useful in investigating the effects of bubble size on mass transfer limited processes operated in the heterogeneous flow regime in bubble columns. Further insights such as the impact of bubble size and the (bubble size dependent) gas-liquid mass transfer coefficient on mass transfer can be obtained

with the proposed model. The importance of accurate parameterizations of the mass, momentum and heat transfer coefficients is emphasized. Size dependent expressions for the mass and heat transfer coefficients will add significant value to the model. Given an accurate estimate of these parameters, model simulations may suggest an optimal bubble size with respect to interfacial mass transfer limitations.

The computational time for this model can be significantly reduced by moving to a faster computer language such as FORTRAN. The extension of the model to 3D coordinates in space and also time is in principle straightforward.

Nomenclature

Latin letters

A	[m^2]	bubble surface area
a_L	[m^2 m^{-3}]	interface area for gas-liquid interface
b	[s^{-1}]	breakage frequency
c	[s^{-1}]	coalescence rate
$\boldsymbol{c}$	[m s^{-1}]	microscopical velocity in spatial space
$\boldsymbol{C}$	[m s^{-1}]	peculiar velocity; $\boldsymbol{C} = \boldsymbol{c} - \boldsymbol{v_r}$
C_{BP}	[-]	bubble pressure proportionality constant
$C_{D,G}$	[-]	drag coefficient
C_L	[-]	lift force coefficient
C_p	[J K^{-1} kg^{-1}]	heat capacity
C_{VM}	[-]	virtual mass force coefficient
$\boldsymbol{C}_s$	[m s^{-1}]	peculiar velocity for a molecule of species s
C_ξ	[m s^{-1}]	peculiar velocity in property space; $C_\xi = \Xi - v_\xi$
$D_{G,z,\text{eff}}$	[m^2 s^{-1}]	effective axial dispersion coefficient
$\boldsymbol{e}$	[-]	unit vector
f	[# m^{-1} m^{-3}]	number density function
f_d	[kg m^{-1} m^{-3}]	mass density function
$\boldsymbol{f}_{\text{drag}}$	[kg m s^{-2} m^{-1}]	drag force
$\boldsymbol{f}_{\text{lift}}$	[kg m s^{-2} m^{-1}]	lift force

$\boldsymbol{f_g}$	[kg m s^{-2} m^{-1}]	gravity force
$\boldsymbol{f_p}$	[kg m s^{-2} m^{-1}]	external pressure force
$\boldsymbol{f}_{TD}$	[kg m s^{-2} m^{-1}]	turbulent dispersion force
$\boldsymbol{f}_{vm}$	[kg m s^{-2} m^{-1}]	virtual mass force
$\boldsymbol{F}_r$	[kg m s^{-2}]	force in physical space
$F_{G,z}$	[kg m s^{-2}]	cross-sectionally averaged force term
F_ξ	[kg m s^{-2}]	force in property space
$\boldsymbol{f}_{\text{drag}}$	[kg m s^{-2} m^{-1}]	drag force
h	[J kg^{-1}]	mass averaged enthalpy
$H(\alpha)$	[-]	dimensionless function in model for bubble pressure
h'	[J kg^{-1}]	fluctuating enthalpy
h_{G-L}	[W m^{-2} K]	gas-liquid heat transfer coefficient
h_p	[J kg^{-1}]	particle enthalpy
h_v	[J kg^{-1}]	specific heat of vaporization
$h_{p,s}$	[J kg^{-1}]	particle specific heat for component s
$\boldsymbol{I}$	[-]	unit tensor
k	[W m^{-1} K^{-1}]	thermal conductivity
$k_{L,s}$	[m s^{-1}]	liquid side mass transfer coefficient for species s
K_s	[-]	weight based vapor-liquid equilibrium constant

m	[kg]	average mass
m_p	[kg]	mass of particle p
$\overline{M_w}$	[kg kmol^{-1}]	average molar mass
p	[m^{-3} m^{-1} s m^{-1} s m^{-1} K^{-1} kg^{-1}]	microscopical number density function
p	[Pa]	pressure
P	[s m^{-1} s m^{-1} K^{-1}]	normalized number density function
$\boldsymbol{P}$	[kg m^{-1} s^{-2}]	pressure tensor
$\boldsymbol{P}_b$	[kg m^{-1} s^{-2}]	bubble pressure tensor
$\boldsymbol{P}_r$	[kg m^{-1} s^{-2}]	viscous stress tensor in spatial space
Pr	[-]	Prandtl number
$\boldsymbol{p}_\xi$	[kg m^{-1} s^{-2}]	viscous stress vector in inner coordinate (bubble diameter) space
$Q_{cd,p}$	[J s^{-1}]	heat exchange for a single particle due to convection and conduction
$Q_{r,p}$	[J s^{-1}]	heat exchange for a single particle due to radiation
$\boldsymbol{q_r}$	[W m^{-2}]	heat flux
$q_{G,z}$	[m^2 s^{-2}]	cross-sectially averaged heat transfer term
q_ξ	[W m^{-2}]	space-property heat flux
$\boldsymbol{r}$	[m]	spatial position
S	[# $[\boldsymbol{q}]^{-1}$]	source term not due to collisions

S_m	[kg m^{-1}m^{-3} s^{-1}]	source term due to coalescence and breakage in the equation of change for mass
$S_{\omega_{s,p}}$	[kg m^{-1}m^{-3} s^{-1}]	source term due to coalescence and breakage in the equation of change for species mass
$S_{\boldsymbol{c}}$	[kg m^{-3} s^{-2}]	source term due to coalescence and breakage in the equation of change for momentum
S_{h_p}	[J m^{-3} m^{-1}]	source term due to coalescence and breakage in the equation of change for enthalpy or temperature
t	[s]	time
T	[K]	temperature
V	[m^3]	volume of particle p
$\boldsymbol{v}$	[m s^{-1}]	velocity
v_z	[m s^{-1}]	cross-sectionally averaged velocity
v_ξ	[m s^{-1}]	growth velocity

Greek letters

α	[-]	volume fraction
γ	[s^{-1}]	mass transfer term (size dependent)
γ_s	[s^{-1}]	mass transfer term (size dependent) for species s

Γ_s	[kg m^{-3} s^{-1}]	mass transfer term for species s
ζ	[m]	diameter of daughter particle
$\lambda_{G,z,\text{eff}}$	[W m^{-1} K^{-1}]	effective turbulent conductivity in spatial space
μ	[Pa s]	viscosity
μ_b	[Pa s]	bulk viscosity
Ξ	[m s^{-1}]	microscopical bubble growth velocity
ξ	[m]	bubble diameter
ρ	[kg m^{-3}]	density
$\boldsymbol{\sigma}$	[kg m^{-1}s^{-2}]	deviatoric stress
$\sigma_{G,z,\text{eff}}$	[kg m^{-1}s^{-2}]	cross-sectionally averged effective (and turbulent) viscous stress for the gas phase
σ_ξ	[kg m^{-1}s^{-2}]	deviatoric stress, property direction
ψ_p	[]	generic particle property
$\omega_{G,s}$	[-]	mass fraction of species s in the gas phase
$\omega_{L,s}$	[-]	mass fraction of species s in the liquid phase
ω_s	[-]	average mass fraction of species s
ω'_s	[-]	fluctuating mass fraction of species s
$\omega_{s,p}$	[-]	mass fraction of species s in particle p

Subscripts

b	bulk
b	bubble
collision	due to collisions
drag	drag
g	gravity
G	gas phase
$G-L$	gas-liquid
in	inlet
lift	lift
L	liquid phase
p	particle
p	pressure
$\boldsymbol{r}$	spatial direction
s	species s
vm	virtual mass
w	weight
ξ	property direction

Superscripts

$*$	at the interface
k	kinetic
T	transposed

620 *Abbreviations*

CM	continuum mechanics
KTGF	kinetic theory of granular flow
MUSIG	multiple size group
PBE	population balance equation
SM	statistical mechanics
FTS	Fischer-Tropsch synthesis
SBC	slurry bubble column

6. Acknowledgments

Helpful communication with Ph.D. Zhongxi Chao regarding the derivation of the equations is acknowledged. The work was supported by the NTNU Department of Chemical Engineering (C. B. Vik) and the Research Council of Norway (J. Solsvik).

References

E. Andresen. *Statistical Approach to Continuum Models for Turbulent Gas-Particle Flows*. PhD thesis, Technical University of Denmark, 1990.

G. K. Batchelor. A new theory on the instability of a uniform fluidized bed. *Journal of Fluid Mechanics*, 193:75–110, 1988.

A. Biesheuvel and W. C. M. Gorissen. Void fraction disturbances in a uniform bubbly fluid. *International Journal of Multiphase Flow*, 16(2):211–231, 1990.

A. Biesheuvel and L. van Wijngaarden. Two-phase flow equations for a dilute dispersion of gas bubbles in a liquid. *Journal of Fluid Mechanics*, 148:301–318, 1984.

A. Buffo, M. Vanni, F. L. Marchisio, and R. O. Fox. Multivariate quadrature-based moments methods for turbulent polydisperse gas-liquid systems. *International Journal of Multiphase Flow*, 50:41–57, 2013.

Z. Chao. *Modeling and Simulation of Reactive Three-phase Flows in Fluidized Bed Reactors: Application to the SE-SMR Process*. PhD thesis, Norwegian University of Science and Technology, 2012.

C. Crowe, J. Schwarzkopf, M. Sommerfeld, and Y. Tsuji. *Multiphase Flows with Droplets and Particles*. Taylor & Francis, Boca Raton, second edition, 2011.

J. de Swart, R. van Vliet, and R. Krishna. Size, structure and dynamics of 'large' bubbles in a two-dimensional slurry bubble column. *Chemical Engineering Science*, 51:4619–4629, 1996.

C. A. Dorao. *High Order Methods for the Solution of the Population Balance Equation with Applications to Bubbly Flows*. PhD thesis, Norwegian University of Science and Technology, 2006.

N. E. L. Haugen, R. E. Mitchell, and M. B. Tilghman. A comprehensive model for char particle conversion in environments containing O_2 and CO_2. *Combustion and Flame*, 162(4):1455–1463, 2015.

J. O. Hirschfelder, C. F. Curtiss, and R. B. Bird. *Molecular Theory of Gases and Liquids*. J. Wiley, New York, 1954.

H. M. Hulburt and S. Katz. Some problems in particle technology: A statistical mechanical formulation. *Chemical Engineering Science*, 19:555–574, 1964.

H. A. Jakobsen. *Chemical Reactor Modeling: Multiphase Reactive Flows*. Springer, Berlin, second edition, 2014.

E. Krepper, D. Lucas, T. Frank, H.-M. Prasser, and P. J. Zwart. The inhomogeneous MUSIG model for the simulation of polydispersed flows. *Nuclear Engineering and Design*, 238:1690–1702, 2008.

660 A. Y. Lafi and J. N. Reyes. General particle transport equation. Technical report,
661 US Department of Energy, 1994.

662 D. Lathouwers and J. Bellan. Modeling of dense gas-solid reactive mixtures applied
663 to biomass pyrolysis in a fluidized bed. In *Proceedings of the 2000 U.S. DOE*
664 *Hydrogen Program Review NREL/CP-570-28890*, 2000.

665 D. Lathouwers and J. Bellan. Modeling of dense gassolid reactive mixtures applied
666 to biomass pyrolysis in a fluidized bed. *International Journal of Multiphase Flow*,
667 27(12):2155–2187, 2001.

668 F. Laurent and M. Massot. Multi-fluid modelling of laminar polydisperse spray
669 flames: origin, assumptions and comparison of sectional and sampling methods.
670 *Combustion Theory and Modelling*, 5:537–572, 2001.

671 Y. Liao and D. Lucas. A literature review on mechanisms and models for the co-
672 alescence process of fluid particles. *Chemical Engineering Science*, 65:2851–2864,
673 2010.

674 H. Lindborg. *Modeling and Simulations of Reactive Two-Phase Flows in Fluidized*
675 *Beds*. PhD thesis, Norwegian University of Science and Technology, 2008.

676 S. Lo. Application of the MUSIG model to bubbly flows. *AEAT -1096, AEA Tech-*
677 *nology*, 1996.

678 D. Lucas, E. Krepper, and H.-M. Prasser. Use of models for lift, wall and turbulent
679 dispersion forces acting on bubbles for poly-disperse flows. *Chemical Engineering*
680 *Science*, 62:4146–4157, 2007.

M. Lysberg, S. Sivakumar, and H. Svendsen. Model studies of three phase methanol synthesis. In *AIChE Annual Meeting, San Fransisco*, 1989.

D. Marchisio and R. Fox. *Computational Models for Polydisperse Particulate and Multiphase Systems*. Cambridge Series in Chemical Engineering. Cambridge University Press, United Kingdom, 2013.

C. Maretto and R. Krishna. Modelling of a bubble column slurry reactor for Fischer-Tropsch synthesis. *Catalysis Today*, 52(2-3):279–289, 1999.

D. Mewes and D. Wiemann. Numerical calculation of mass transfer with heterogeneous chemical reactions in three-phase bubble columns. In *Proceedings of FEDSM2007 5th Joint ASME/JSME Fluids Engineering Conference*, 2007.

M. Millies and D. Mewes. Phasengrenzflächen in blasenströmungen – teil 1: Blasensäulen. *Chemie Ingenieur Technik*, 68:660–669, 1996.

S. M. Monahan. *Computational fluid dynamics analysis of air-water bubble columns*. PhD thesis, Iowa State Universty, 2007.

C. Morel. *Mathematical Modeling of Disperse Two-Phase Flows*. Springer, New York, 2015.

A. Nayak, Z. Borka, L. Patruno, F. Sporleder, C. Dorao, and H. Jakobsen. A combined multifluid-population balance model for vertical gas-liquid bubble-driven flows considering bubble column operating conditions. *Industrial & Engineering Chemistry Research*, 50(3):1786–1798, 2011.

L. E. Patruno. *Experimental and Numerical Investigations of Liquid Fragmentation and Droplet Generation for Gas Processing at High Pressures.* PhD thesis, Norwegian University of Science and Technology, 2010.

D. Ramkrishna. *Population Balances: Theory and Applications to Particulate Systems in Engineering.* Academic Press, San Diego, 2000.

A. D. Randolph. A population balance for countable entities. *The Canadian Journal of Chemical Engineering*, 42(6):280–281, 1964.

A. D. Randolph and M. A. Larson. *Theory of Particulate Processes.* Academic Press, San Diego, second edition, 1988.

J. N. Reyes. Statistically derived conservation equations for fluid particle flows. *Transactions of the American Nuclear Society*, 60:669–672, 1989.

K. Sankaranarayanan and S. Sundaresan. Lift force in bubbly suspensions. *Chemical Engineering Science*, 52:3521–3542, 2002.

S. Seetharaman. *Treatise on Process Metallurgy, Volume 3: Industrial Processes.* Treatise on Process Metallurgy. Elsevier Science, 2013.

Q. Segers. *Cutting Bubbles using Wire-Mesh Structures – Direct Numerical Simulations.* PhD thesis, TU Eindhoven, 2015.

L. Sehabiague, R. Lemoine, A. Behkish, Y. J. Heintz, M. Sanoja, R. Oukaci, and B. I. Morsi. Modeling and optimization of a large-scale slurry bubble column reactor for producing 10,000 bbl/day of Fischer-Tropsch liquid hydrocarbons. *Journal of the Chinese Institute of Chemical Engineers*, 39(2):169–179, 2008.

O. Simonin. Continuum modelling of dispersed two-phase flows. In *Combustion and turbulence in two-phase flows*, volume 2, pages 1–47. van Karman Institute for fluid dynamics, 1996.

J. Solsvik and H. A. Jakobsen. Evaluation of weighted residual methods for the solution of a population balance model describing bubbly flows: The least-squares, galerkin, tau, and orthogonal colnote methods. *Industrial & Engineering Chemistry Research*, 52(45):15988–16013, 2013.

J. Solsvik and H. A. Jakobsen. A combined multifluid-population balance model applied to dispersed gas-liquid flows. *Journal for Dispersion Science and Technology*, 35:1611–1625, 2014a.

J. Solsvik and H. A. Jakobsen. The foundation of the population balance equation – a review. *Journal of Dispersion Science and Technology*, 36:510–520, 2014b.

J. Solsvik and H. A. Jakobsen. A review of the concepts for deriving the equations of change for the classical kinetic theory of gases: Single-component, multicomponent and reactive gases. *European Journal of Mechanics B/Fluids*, 56:46–65, 2016.

J. Solsvik, S. Tangen, and H. A. Jakobsen. On the constitutive equations for fluid particle breakage. *Reviews in Chemical Engineering*, 29:241–356, 2013.

P. D. M. Spelt and A. S. Sangani. Properties and averaged equations for flows of bubbly liquids. *Applied Scientific Research*, 58:337–386, 1998.

F. Sporleder, Z. Borka, J. Solsvik, and H. Jakobsen. On the population balance equation. *Reviews in Chemical Engineering*, 28(2-3):149–169, 2012.

C. B. Vik, J. Solsvik, M. Hillestad, and H. A. Jakobsen. Modeling of a slurry bubble column reactor for the production of biofuels via the Fischer-Tropsch synthesis. *Chemical Engineering & Technology*, 38(4):690–700, 2015.

F. A. Williams. Spray combustion and atomization. *Physics of Fluids*, 1:541–545, 1958.

Z. Zhu. *The Least-Squares Spectral Element Method Solution of the Gas-Liquid Multi-fluid Model Coupled with the Population Balance Equation*. PhD thesis, Norwegian University of Science and Technology, 2009.

Table 1: Reactor dimensions and operating conditions for the FTS operated in a SBC at industrial conditions. Further details are given in Vik et al. (2015).

Reactor height	50	m
Reactor diameter	9	m
Outlet pressure	30	bar
Inlet temperature	513	K
Inlet H_2/CO molar ratio	2	-
Inlet weight fraction of CO_2	0.1	-
Inlet gas superficial velocity	0.26	m/s
Inlet solid superficial velocity	0.01	m/s
Inlet liquid superficial velocity	0.01	m/s
Inlet gas volume fraction	0.50	-
Inlet liquid volume fraction	0.47	-
Inlet solid volume fraction	0.03	-
Bubble size domain	0.1 - 55	mm
Inlet Sauter mean diameter	10	mm
Catalyst loading	35	wt cat / wt slurry

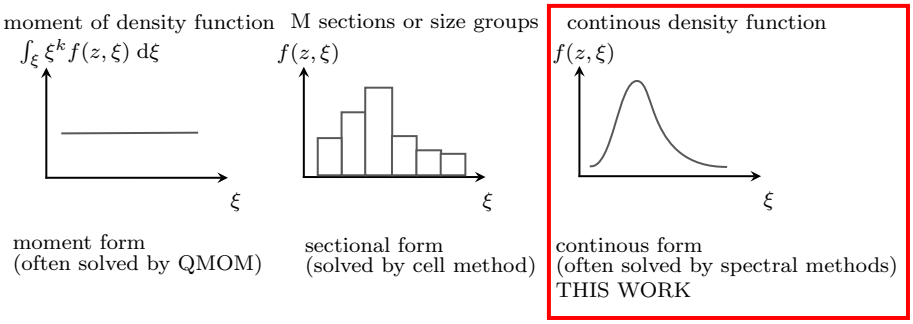

Figure 1: Number density functions for the moment form, sectional form and continuous form of the PBE.

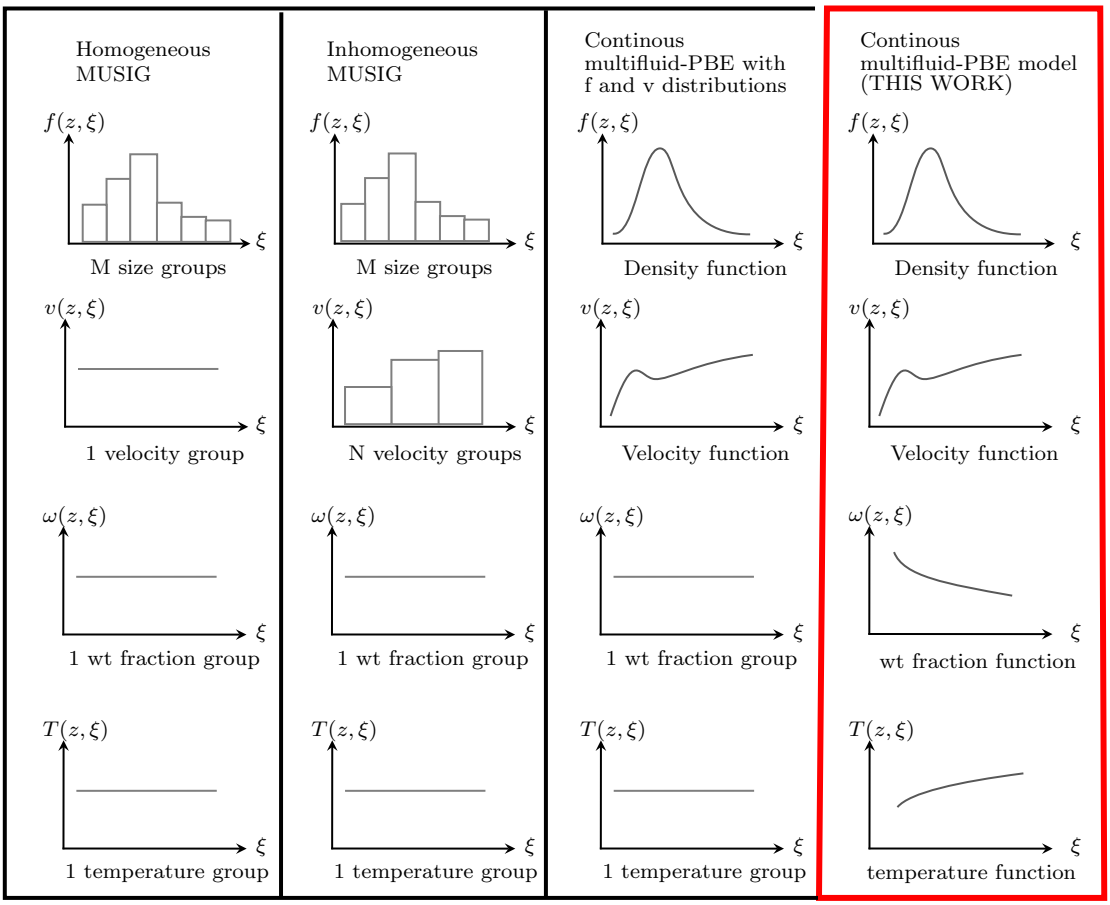

Figure 2: Distinction between sectional and continuous multifluid-PBE models. The moment form of PBE is not shown here.

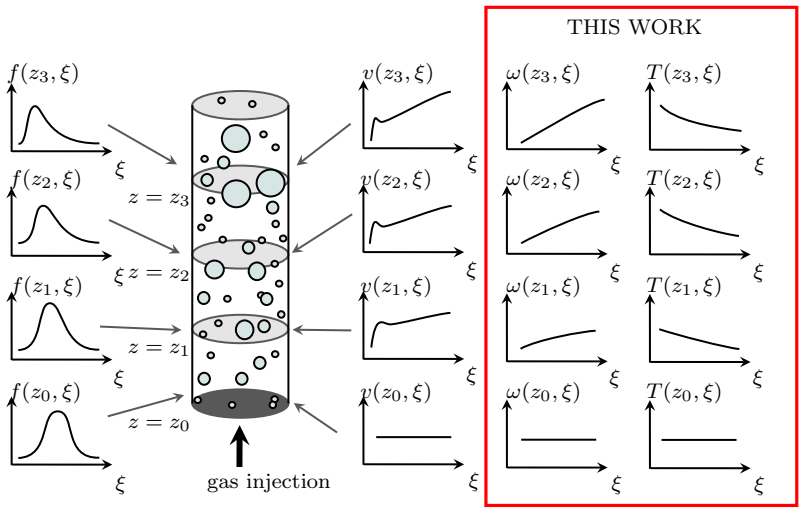

Figure 3: Velocity, weight fraction and temperature for the dispersed phase are continuous functions of ξ - here shown for different levels of z. Based on Dorao (2006).

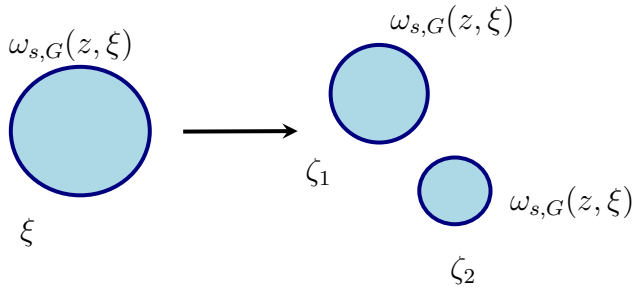

Figure 4: Binary breakage of one spherical mother bubble (left) into two spherical daughter bubbles (right) on the particle level.

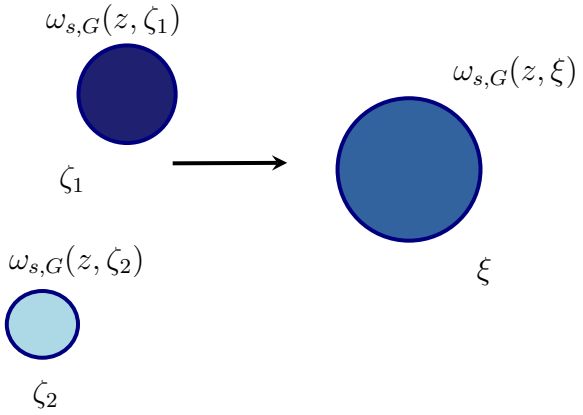

Figure 5: Binary coalescence of two spherical mother bubbles (left) into one spherical daughter bubble (right) on the particle level.

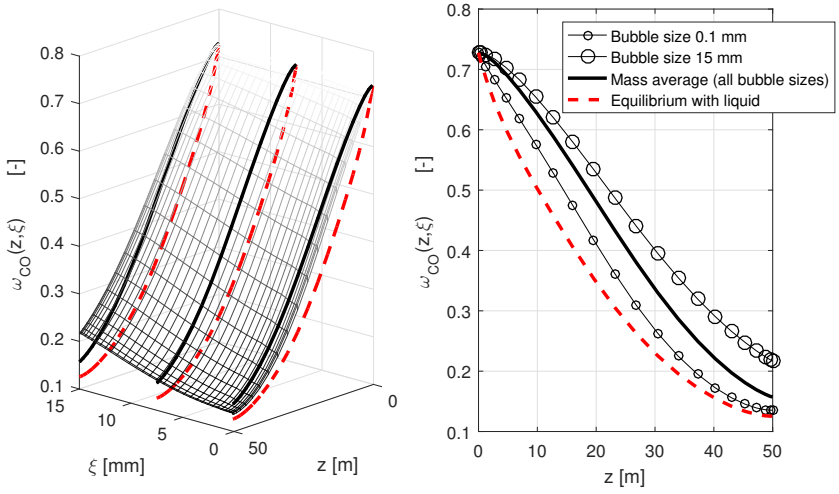

Figure 6: Dispersed phase weight fractions as function of bubble size and axial direction.

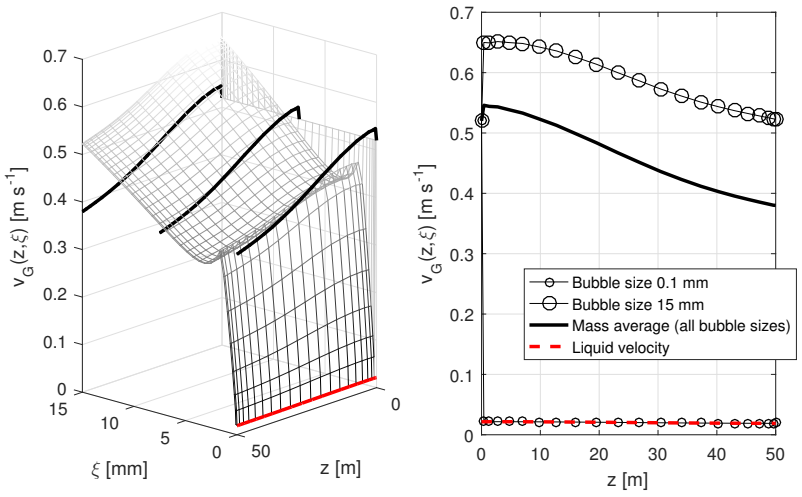

Figure 7: Dispersed phase velocity as function of bubble size and axial direction.

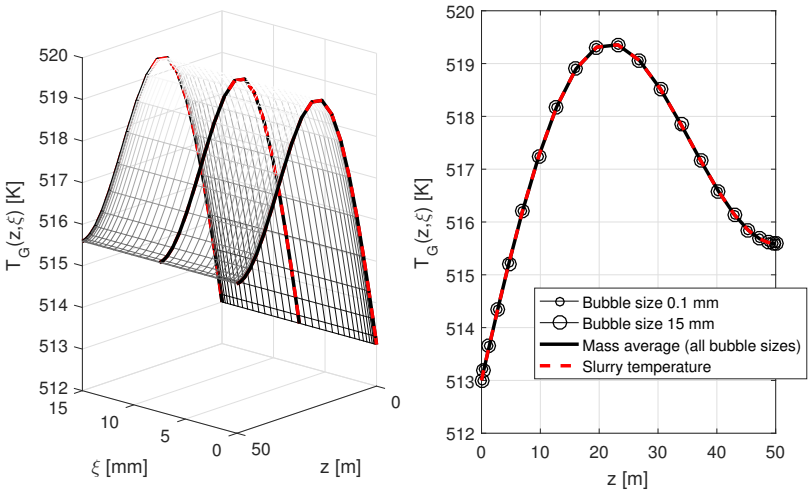

Figure 8: Bubble temperature as function of bubble size and axial direction.

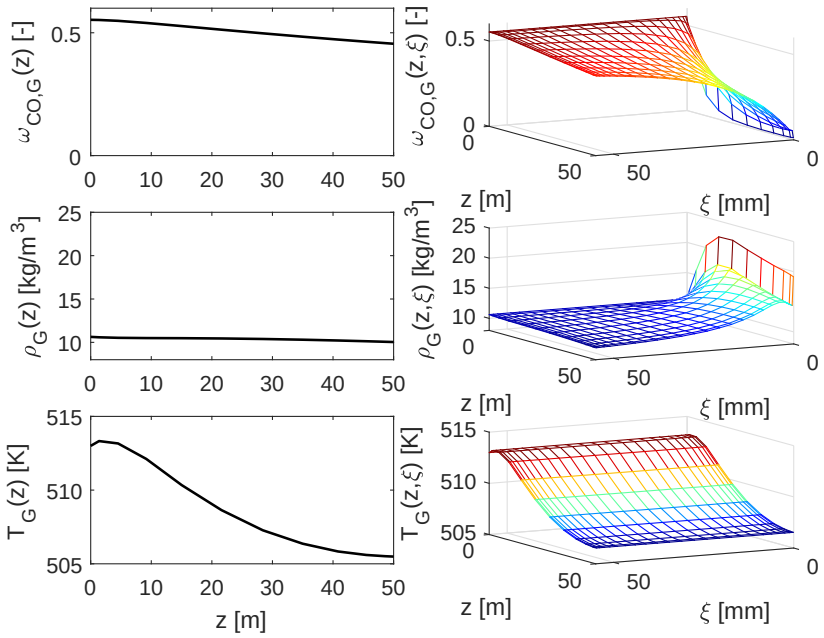

Figure 9: Comparison of composition, density and temperature profiles for the existing model (Vik et al., 2015) and the proposed model.

Appendix A. Derivation of the moment equation

This section shows the derivation of a macroscopic or moment equation for the generic property $\langle\psi_p\rangle$. To derive the moment equation for a generic particle property ψ_p we multiply the Boltzmann-like equation (Eq. 22) with ψ_p and integrate over all velocities, the weight fraction, temperature and the mass of the particle (as in Lathouwers and Bellan (2000)), but not the bubble size ξ, to obtain

$$\begin{aligned}
&\int_{-\infty}^{+\infty} m_p\psi_p\frac{\partial p}{\partial t}\,\mathrm{d}\Omega + \int_{-\infty}^{+\infty} m_p\psi_p\boldsymbol{c}\cdot\frac{\partial p}{\partial \boldsymbol{r}}\,\mathrm{d}\Omega \\
&+ \int_{-\infty}^{+\infty} m_p\psi_p\boldsymbol{F_r}\cdot\frac{\partial p}{\partial \boldsymbol{c}}\,\mathrm{d}\Omega + \int_{-\infty}^{+\infty} m_p\psi_p\Xi\frac{\partial p}{\partial \xi}\,\mathrm{d}\Omega + \int_{-\infty}^{+\infty} m_p\psi_p F_\xi\frac{\partial p}{\partial \Xi}\,\mathrm{d}\Omega \\
&+ \int_{-\infty}^{+\infty} m_p\psi_p\dot{T}_p\frac{\partial p}{\partial T_p}\,\mathrm{d}\Omega + \sum_s\int_{-\infty}^{+\infty} m_p\psi_p\dot{\omega}_{s,p}\frac{\partial p}{\partial \omega_{s,p}}\,\mathrm{d}\Omega \\
&+ \int_{-\infty}^{+\infty} m_p\psi_p\dot{m}_p\frac{\partial p}{\partial m_p}\,\mathrm{d}\Omega = \int_{-\infty}^{+\infty} m_p\psi_p\left(\frac{\partial p}{\partial t}\right)_{\mathrm{coll}}\,\mathrm{d}\Omega + \int_{-\infty}^{+\infty} m_p S\,\mathrm{d}\Omega
\end{aligned} \tag{A.1}$$

where we have written $\mathrm{d}\Omega = d\boldsymbol{c}d\Xi\,\mathrm{d}\omega_{s,p}dT_p dm_p$ for brevity (as in Chao (2012)). For the first term:

$$\begin{aligned}
&\int_{-\infty}^{+\infty} m_p\psi_p\frac{\partial p}{\partial t}\,\mathrm{d}\Omega \\
&= \int_{-\infty}^{+\infty}\left[\frac{\partial}{\partial t}(m_p\psi_p p) - m_p p\frac{\partial \psi_p}{\partial t} - \psi_p p\frac{\partial m_p}{\partial t}\right]\,\mathrm{d}\Omega \\
&= \frac{\partial}{\partial t}\int_{-\infty}^{+\infty} m_p\psi_p p\,\mathrm{d}\Omega - \int_{-\infty}^{+\infty} m_p p\frac{\partial \psi_p}{\partial t}\,\mathrm{d}\Omega \\
&= \frac{\partial}{\partial t}(f_d\langle\psi_p\rangle) - f_d\langle m_p\frac{\partial \psi_p}{\partial t}\rangle
\end{aligned} \tag{A.2}$$

by writing out the total differential and utilizing Eq. 7. We have realized that m_p as a coordinate is independent of all other coordinates, including t. The microscopical number density function p is assumed to go to zero as $\omega \to -\infty$ and $\omega \to +\infty$. For the second term:

$$\begin{aligned}
&\int_{-\infty}^{+\infty} m_p \boldsymbol{c} \psi_p \cdot \frac{\partial p}{\partial \boldsymbol{r}} \, \mathrm{d}\Omega \\
&= \int_{-\infty}^{+\infty} \left[\frac{\partial}{\partial \boldsymbol{r}} \cdot (m_p \psi_p p \boldsymbol{c}) - m_p p \boldsymbol{c} \cdot \frac{\partial \psi_p}{\partial \boldsymbol{r}} - p \boldsymbol{c} \psi_p \cdot \frac{\partial m_p}{\partial \boldsymbol{r}} - m_p \psi_p p \frac{\partial \boldsymbol{c}}{\partial \boldsymbol{r}} \right] \, \mathrm{d}\Omega \\
&= \frac{\partial}{\partial \boldsymbol{r}} \cdot \int_{-\infty}^{+\infty} m_p \psi_p p \boldsymbol{c} \, \mathrm{d}\Omega - \int_{-\infty}^{+\infty} m_p p \boldsymbol{c} \cdot \frac{\partial \psi_p}{\partial t} \, \mathrm{d}\Omega \\
&= \frac{\partial}{\partial \boldsymbol{r}} \cdot (f_d \langle \psi_p \boldsymbol{c} \rangle) - f_d \langle \boldsymbol{c} \cdot \frac{\partial \psi_p}{\partial \boldsymbol{r}} \rangle
\end{aligned} \tag{A.3}$$

where we have utilized Eq. 7 and realized m_p and $\boldsymbol{c}$ are independent of $\boldsymbol{r}$. For the force term, the third term in Eq. A.1:

$$\begin{aligned}
&\int_{-\infty}^{+\infty} m_p \psi_p \boldsymbol{F_r} \cdot \frac{\partial p}{\partial \boldsymbol{c}} \, \mathrm{d}\Omega \\
&= \int_{-\infty}^{+\infty} \left[\frac{\partial}{\partial \boldsymbol{c}} \cdot (m_p \psi_p p \boldsymbol{F_r}) - m_p p \boldsymbol{F_r} \cdot \frac{\partial \psi_p}{\partial \boldsymbol{c}} - p \psi_p \boldsymbol{F_r} \cdot \frac{\partial m_p}{\partial \boldsymbol{c}} - m_p \psi_p p \frac{\partial \boldsymbol{F_r}}{\partial \boldsymbol{c}} \right] \, \mathrm{d}\Omega \\
&= [m_p \psi_p p \boldsymbol{F_r}]_{-\infty}^{+\infty} - \int_{-\infty}^{+\infty} m_p p \boldsymbol{F_r} \cdot \frac{\partial \psi_p}{\partial \boldsymbol{c}} \, \mathrm{d}\Omega \\
&= -f_d \langle \boldsymbol{F_r} \cdot \frac{\partial \psi_p}{\partial \boldsymbol{c}} \rangle
\end{aligned} \tag{A.4}$$

765 as m_p and $\boldsymbol{F_r}$ are independent of $\boldsymbol{c}$ and $p \to 0$ as $\omega \to -\infty, +\infty$. For the fourth
766 term:

$$
\begin{aligned}
&\int_{-\infty}^{+\infty} m_p \psi_p \Xi \frac{\partial p}{\partial \xi} \, \mathrm{d}\Omega \\
&= \int_{-\infty}^{+\infty} \left[\frac{\partial}{\partial \xi}(m_p \psi_p \Xi p) - m_p p \Xi \frac{\partial \psi_p}{\partial \xi} - p \psi_p \Xi \frac{\partial m_p}{\partial \xi} - m_p p \psi_p \frac{\partial \Xi}{\partial \xi} \right] \, \mathrm{d}\Omega \\
&= \int_{-\infty}^{+\infty} \frac{\partial}{\partial \xi}(m_p \psi_p \Xi p) \, \mathrm{d}\Omega - \int_{-\infty}^{+\infty} m_p p \Xi \frac{\partial \psi_p}{\partial \xi} \, \mathrm{d}\Omega \\
&= \frac{\partial}{\partial \xi} \int_{-\infty}^{+\infty} (m_p \psi_p \Xi p) \, \mathrm{d}\Omega - \int_{-\infty}^{+\infty} m_p p \Xi \frac{\partial \psi_p}{\partial \xi} \, \mathrm{d}\Omega \\
&= \frac{\partial}{\partial \xi} \langle \Xi \psi_p \rangle - f_d \langle \Xi \frac{\partial \psi_p}{\partial \xi} \rangle
\end{aligned}
\tag{A.5}
$$

767 as Ξ is independent of ξ. For the fifth term:

$$
\begin{aligned}
&\int_{-\infty}^{+\infty} m_p \psi_p F_\xi \frac{\partial p}{\partial \xi} \, \mathrm{d}\Omega \\
&= \int_{-\infty}^{+\infty} \left[\frac{\partial}{\partial \Xi}(m_p \psi_p F_\xi p) - m_p p F_\xi \frac{\partial \psi_p}{\partial \Xi} - p \psi_p F_\xi \frac{\partial m_p}{\partial \Xi} - m_p p \psi_p \frac{\partial F_\xi}{\partial \Xi} \right] \, \mathrm{d}\Omega \\
&= \int_{-\infty}^{+\infty} \frac{\partial}{\partial \Xi}(m_p \psi_p F_\xi p) \, \mathrm{d}\Omega - \int_{-\infty}^{+\infty} m_p p F_\xi \frac{\partial \psi_p}{\partial \Xi} \, \mathrm{d}\Omega \\
&= [m_p \psi_p F_\xi p]_{-\infty}^{+\infty} - \int_{-\infty}^{+\infty} m_p p F_\xi \frac{\partial \psi_p}{\partial \Xi} \, \mathrm{d}\Omega \\
&= -f_d \langle F_\xi \frac{\partial \psi_p}{\partial \Xi} \rangle
\end{aligned}
\tag{A.6}
$$

as m_p and F_ξ are independent of Ξ. For the sixth term:

$$\begin{aligned}
&\int_{-\infty}^{+\infty} m_p \psi_p \dot{T}_p \frac{\partial p}{\partial T_p} \, \mathrm{d}\Omega \\
&= \int_{-\infty}^{+\infty} \left[\frac{\partial}{\partial T_p}(m_p \psi_p \dot{T}_p p) - m_p \dot{T}_p p \frac{\partial \psi_p}{\partial T_p} - \psi_p \dot{T}_p p \frac{\partial m_p}{\partial T_p} - m_p \psi_p p \frac{\partial \dot{T}_p}{\partial T_p} \right] \, \mathrm{d}\Omega \\
&= [m_p \psi_p \dot{T}_p p]_{-\infty}^{+\infty} - \int_{-\infty}^{+\infty} m_p \dot{T}_p p \frac{\partial \psi_p}{\partial T_p} \, \mathrm{d}\Omega \\
&= -f_d \langle \dot{T}_p \frac{\partial \psi_p}{\partial T_p} \rangle
\end{aligned} \tag{A.7}$$

as m_p, $\dot{T}_p$ are independent of T_p. For the seventh term:

$$\begin{aligned}
&\sum_s \int_{-\infty}^{+\infty} m_p \psi_p \dot{\omega}_{s,p} \frac{\partial p}{\partial \omega_{s,p}} \, \mathrm{d}\Omega \\
&= \sum_s \int_{-\infty}^{+\infty} \left[\frac{\partial}{\partial \omega_{s,p}}(m_p \psi_p \dot{\omega}_{s,p} p) - m_p \dot{\omega}_{s,p} p \frac{\partial \psi_p}{\partial \omega_{s,p}} \right] \, \mathrm{d}\Omega + \\
&\quad \sum_s \int_{-\infty}^{+\infty} \left[-\psi_p \dot{\omega}_{s,p} p \frac{\partial m_p}{\partial \omega_{s,p}} - m_p \psi_p p \frac{\partial \dot{\omega}_{s,p}}{\partial \omega_{s,p}} \right] \, \mathrm{d}\Omega \\
&= \sum_s [m_p \psi_p \dot{\omega}_{s,p} p]_{-\infty}^{+\infty} - \sum_s \int_{-\infty}^{+\infty} m_p \dot{\omega}_{s,p} p \frac{\partial \psi_p}{\partial \omega_{s,p}} \, \mathrm{d}\Omega \\
&= -f_d \sum_s \langle \dot{\omega}_{s,p} \frac{\partial \psi_p}{\partial \omega_{s,p}} \rangle
\end{aligned} \tag{A.8}$$

as m_p, $\dot{\omega}_{s,p}$ are independent of $\omega_{s,p}$. For the eighth term:

$$
\begin{aligned}
&\int_{-\infty}^{+\infty} m_p \psi_p \dot{m}_p \frac{\partial p}{\partial m_p} \, \mathrm{d}\Omega \\
&= \int_{-\infty}^{+\infty} \left[\frac{\partial}{\partial m_p}(m_p \psi_p \dot{m}_p p) - p m_p \dot{m}_p \frac{\partial \psi_p}{\partial m_p} - p \dot{m}_p \psi_p \frac{\partial m_p}{\partial m_p} - p \psi_p m_p \frac{\partial \dot{m}_p}{\partial m_p} \right] \, \mathrm{d}\Omega \\
&= [m_p \psi_p \dot{m}_p p]_{-\infty}^{+\infty} - \int_{-\infty}^{+\infty} p m_p \dot{m}_p \frac{\partial \psi_p}{\partial m_p} \, \mathrm{d}\Omega - \int_{-\infty}^{+\infty} p \dot{m}_p \psi_p \, \mathrm{d}\Omega \\
&= -f_d \langle \dot{m}_p \frac{\partial \psi_p}{\partial m_p} \rangle - \int_{-\infty}^{+\infty} p \dot{m}_p \frac{m_p}{m_p} \psi_p \, \mathrm{d}\Omega \\
&= -f_d \langle \dot{m}_p \frac{\partial \psi_p}{\partial m_p} \rangle - f_d \langle \frac{\dot{m}_p}{m_p} \psi_p \rangle \\
&= -f_d \langle \dot{m}_p \left(\frac{\partial \psi_p}{\partial m_p} + \frac{\psi}{m_p} \right) \rangle
\end{aligned}
\tag{A.9}
$$

The ninth and tenth terms are combined to a source term denoted $\langle S_{\psi_p} \rangle$. Combining all terms gives the moment equation:

$$
\begin{aligned}
&\frac{\partial}{\partial t}(f_d \langle \psi_p \rangle + \frac{\partial}{\partial \boldsymbol{r}} \cdot (f_d \langle \psi_p \boldsymbol{c} \rangle) + \frac{\partial}{\partial \xi}(f_d \langle \Xi \psi_p \rangle) = \\
&f_d \left[\langle \frac{\partial \psi_p}{\partial t} \rangle + \langle \boldsymbol{c} \cdot \frac{\partial \psi_p}{\partial \boldsymbol{r}} \rangle + \langle \boldsymbol{F_r} \cdot \frac{\partial \psi_p}{\partial \boldsymbol{c}} \rangle + \langle \Xi \frac{\partial \psi_p}{\partial \xi} \rangle + \langle F_\xi \frac{\partial \psi_p}{\partial \Xi} \rangle \right] \\
&+ f_d \left[\langle \dot{T}_p \frac{\partial \psi_p}{\partial T_p} \rangle + \sum_s \langle \dot{\omega}_{s,p} \frac{\partial \psi_p}{\partial \omega_{s,p}} \rangle + \langle \dot{m}_p \left(\frac{\partial \psi_p}{\partial m_p} + \frac{\psi_p}{m_p} \right) \rangle \right] \\
&+ \langle S_{\psi_p} \rangle
\end{aligned}
\tag{A.10}
$$

Appendix B. Derivation of the dispersed phase equations

Appendix B.1. Mass

The equation of change for mass is obtained by inserting for $\psi_p = 1$ into Eq. (23). This gives:

$$\frac{\partial f_d\langle 1\rangle}{\partial t} + \frac{\partial}{\partial \boldsymbol{r}} \cdot (f_d\langle \boldsymbol{c}1\rangle) + \frac{\partial}{\partial \xi}(f_d\langle \Xi 1\rangle) = f_d\langle \frac{\mathrm{d}m_p}{\mathrm{d}t}\left(\frac{1}{m_p}\right)\rangle + \langle S_1\rangle \tag{B.1}$$

where all terms on the right hand side of Eq. (23) except two terms disappear as the derivative of the scalar 1 is zero. For the left hand side we insert for Eq. (10) and Eq. (12) and obtain the conservation equation for mass:

$$\frac{\partial f_d}{\partial t} + \frac{\partial}{\partial \boldsymbol{r}} \cdot (f_d \boldsymbol{v_r}) + \frac{\partial}{\partial \xi}(f_d v_\xi) = f_d\langle \frac{\mathrm{d}m_p}{\mathrm{d}t}\left(\frac{1}{m_p}\right)\rangle + \langle S_1\rangle \tag{B.2}$$

Eq. (24) is a PBE formulated in terms of a mass density function f_d. It describes the evolution of the mass of bubbles in phase space.

Appendix B.2. Species mass

The equation of change for species mass is obtained by inserting for $\psi_p = \omega_{s,p}$ into Eq. (23):

$$\begin{aligned} &\frac{\partial f_d\langle \omega_{s,p}\rangle}{\partial t} + \frac{\partial}{\partial \boldsymbol{r}} \cdot (f_d\langle \boldsymbol{c}\omega_{s,p}\rangle) + \frac{\partial}{\partial \xi}(f_d\langle \Xi\omega_{s,p}\rangle) = \\ &f_d\left[\langle \frac{\mathrm{d}\omega_{s,p}}{\mathrm{d}t}\rangle + \langle \frac{\mathrm{d}m_p}{\mathrm{d}t}\left(\frac{\omega_{s,p}}{m_p}\right)\rangle\right] + \langle S_{\omega_{s,p}}\rangle \end{aligned} \tag{B.3}$$

For the transient term we utilize Eq. (14):

$$\frac{\partial f_d \langle \omega_{s,p} \rangle}{\partial t} = \frac{\partial (f_d \omega_s)}{\partial t} \tag{B.4}$$

For the convection term in physical space we decompose the velocities and weight fractions into a mean and fluctuating term according to Eq. (11) and Eq. (16) and utilize Eq. (14):

$$\begin{aligned}
\frac{\partial}{\partial \boldsymbol{r}} \cdot (f_d \langle \boldsymbol{c} \omega_{s,p} \rangle) &= \frac{\partial}{\partial \boldsymbol{r}} \cdot (f_d \langle (\boldsymbol{v_r} + \boldsymbol{C})(\omega_s + \omega_s') \rangle) \\
&= \frac{\partial}{\partial \boldsymbol{r}} \cdot (f_d \langle \boldsymbol{v_r} \omega_s + \boldsymbol{C} \omega_s + \boldsymbol{v_r} \omega_s' + \boldsymbol{C} \omega_s' \rangle) \\
&= \frac{\partial}{\partial \boldsymbol{r}} \cdot (f_d \boldsymbol{v_r} \langle \omega_s \rangle) + \frac{\partial}{\partial \boldsymbol{r}} \cdot (f_d \langle \boldsymbol{C} \omega_s' \rangle) \\
&= \frac{\partial}{\partial \boldsymbol{r}} \cdot (f_d \boldsymbol{v_r} \omega_s) + \frac{\partial}{\partial \boldsymbol{r}} \cdot (f_d \langle \boldsymbol{C} \omega_s' \rangle)
\end{aligned} \tag{B.5}$$

and for the convection in property space we apply Eq. (13), Eq. (14) and Eq. (16):

$$\begin{aligned}
\frac{\partial}{\partial \xi} (f_d \langle \Xi \omega_{s,p} \rangle) &= \frac{\partial}{\partial \xi} (f_d \langle (v_\xi + C_\xi)(\omega_s + \omega_s') \rangle) \\
&= \frac{\partial}{\partial \xi} (f_d \langle v_\xi \omega_s + C_\xi \omega_s + v_\xi \omega_s' + C_\xi \omega_s' \rangle) \\
&= \frac{\partial}{\partial \xi} (f_d v_\xi \langle \omega_s \rangle) + \frac{\partial}{\partial \xi} (f_d \langle C_\xi \omega_s' \rangle) \\
&= \frac{\partial}{\partial \xi} (f_d v_\xi \omega_s) + \frac{\partial}{\partial \xi} (f_d \langle C_\xi \omega_s' \rangle)
\end{aligned} \tag{B.6}$$

To evaluate the terms on the right hand side of Eq. (B.3) we consider single particle dynamics for a bubble. The mass transfer for component s in a bubble is given

by Lathouwers and Bellan (2000):

$$\frac{\mathrm{d}m_{s,p}}{\mathrm{d}t} = \frac{\mathrm{d}(m_p\omega_{s,p})}{\mathrm{d}t} = m_p\frac{\mathrm{d}\omega_{s,p}}{\mathrm{d}t} + \omega_{s,p}\frac{\mathrm{d}m_p}{\mathrm{d}t} \tag{B.7}$$

Expressing Eq. (B.7) in terms of $\frac{\mathrm{d}\omega_{s,p}}{\mathrm{d}t}$:

$$\frac{\mathrm{d}\omega_{s,p}}{\mathrm{d}t} = \frac{1}{m_p}\left[\frac{\mathrm{d}m_{s,p}}{\mathrm{d}t} - \omega_{s,p}\frac{\mathrm{d}m_p}{\mathrm{d}t}\right] \tag{B.8}$$

Inserting Eq. (B.8) into the two mass transfer terms in the right hand side of Eq. (B.3) gives:

$$\begin{aligned} &f_d\langle\frac{1}{m_p}\left[\frac{\mathrm{d}m_{s,p}}{\mathrm{d}t} - \omega_{s,p}\frac{\mathrm{d}m_p}{\mathrm{d}t}\right] + \frac{\mathrm{d}m_p}{\mathrm{d}t}\frac{\omega_{s,p}}{m_p}\rangle \\ &= f_d\langle\frac{1}{m_p}\frac{\mathrm{d}m_{s,p}}{\mathrm{d}t}\rangle \end{aligned} \tag{B.9}$$

Combining the terms gives the equation of change for species mass:

$$\begin{aligned} &\frac{\partial(f_d\omega_s)}{\partial t} + \frac{\partial}{\partial \boldsymbol{r}}\cdot(f_d\boldsymbol{v}_{\boldsymbol{r}}\omega_s) + \frac{\partial}{\partial\xi}(f_d v_\xi\omega_s) \\ &= -\frac{\partial}{\partial \boldsymbol{r}}\cdot(f_d\langle\boldsymbol{C}\omega_s'\rangle) - \frac{\partial}{\partial\xi}(f_d\langle C_\xi\omega_s'\rangle) + f_d\langle\frac{1}{m_p}\frac{dm_{s,p}}{\mathrm{d}t}\rangle + \langle S_{\omega_{s,p}}\rangle \end{aligned} \tag{B.10}$$

Appendix B.3. Momentum

The equation of change for momentum is found by inserting for $\psi_p = \boldsymbol{c}$ into Eq. (23):

$$\frac{\partial(f_d\langle\boldsymbol{c}\rangle)}{\partial t} + \frac{\partial}{\partial \boldsymbol{r}}\cdot(f_d\langle\boldsymbol{c}\boldsymbol{c}\rangle) + \frac{\partial}{\partial\xi}(f_d\langle\Xi\boldsymbol{c}\rangle) = f_d\langle\boldsymbol{F}_{\boldsymbol{r}}\cdot\frac{\partial\boldsymbol{c}}{\partial\boldsymbol{c}}\rangle + f_d\langle\frac{\mathrm{d}m_p}{\mathrm{d}t}\frac{\boldsymbol{c}}{m_p}\rangle + \langle S_{\boldsymbol{c}}\rangle \tag{B.11}$$

For the transient term we use Eq. (10):

$$\frac{\partial(f_d\langle \boldsymbol{c}\rangle)}{\partial t} = \frac{\partial(f_d \boldsymbol{v_r})}{\partial t} \tag{B.12}$$

For the convective term in physical space we decompose the spatial velocity according to Eq. (11):

$$\begin{aligned}
\frac{\partial}{\partial \boldsymbol{r}} \cdot (f_d\langle \boldsymbol{cc}\rangle) &= \frac{\partial}{\partial \boldsymbol{r}} \cdot (f_d\langle (\boldsymbol{v_r}+\boldsymbol{C})(\boldsymbol{v_r}+\boldsymbol{C})\rangle) \\
&= \frac{\partial}{\partial \boldsymbol{r}} \cdot (f_d\langle \boldsymbol{v_r v_r} + 2\boldsymbol{C v_r} + \boldsymbol{CC}\rangle) \\
&= \frac{\partial}{\partial \boldsymbol{r}} \cdot (f_d\langle \boldsymbol{v_r v_r}\rangle) + 2\frac{\partial}{\partial \boldsymbol{r}} \cdot (f_d\langle \boldsymbol{C v_r}\rangle) + \frac{\partial}{\partial \boldsymbol{r}} \cdot (f_d\langle \boldsymbol{CC}\rangle) \\
&= \frac{\partial}{\partial \boldsymbol{r}} \cdot (f_d \boldsymbol{v_r v_r}) + \frac{\partial}{\partial \boldsymbol{r}} \cdot \boldsymbol{P_r}
\end{aligned} \tag{B.13}$$

where $\boldsymbol{P_r} = f_d\langle \boldsymbol{CC}\rangle$ is the pressure tensor (Eq. (18)). For the convective term in the property space we decompose the velocity according to Eq. (13):

$$\begin{aligned}
\frac{\partial}{\partial \xi}(f_d\langle \Xi \boldsymbol{c}\rangle) &= \frac{\partial}{\partial \xi}(f_d\langle (v_\xi + C_\xi)(\boldsymbol{v_r}+\boldsymbol{C})\rangle) \\
&= \frac{\partial}{\partial \xi}(f_d\langle v_\xi \boldsymbol{v_r} + v_\xi \boldsymbol{C} + C_\xi \boldsymbol{v_r} + C_\xi \boldsymbol{C}\rangle) \\
&= \frac{\partial}{\partial \xi}(f_d v_\xi \boldsymbol{v_r}) + \frac{\partial}{\partial \xi}(f_d\langle v_\xi \boldsymbol{C}\rangle) + \frac{\partial}{\partial \xi}(f_d\langle C_\xi \boldsymbol{v_r}\rangle) + \frac{\partial}{\partial \xi}(f_d\langle C_\xi \boldsymbol{C}\rangle) \\
&= \frac{\partial}{\partial \xi}(f_d v_\xi \boldsymbol{v_r}) + \frac{\partial}{\partial \xi}\boldsymbol{p_\xi}
\end{aligned} \tag{B.14}$$

where $\boldsymbol{p_\xi} = f_d\langle C_\xi \boldsymbol{C}\rangle$ is the bubble space-property pressure vector (Eq. (20)).

For the force term we use a force balance for a single particle as shown by Lathouwers and Bellan (2000) combined with additional forces relevant for bubbly flow (Jakobsen,

2014):

$$f_d\langle \boldsymbol{F_r} \cdot \frac{\partial \boldsymbol{c}}{\partial \boldsymbol{c}} \rangle = f_d\langle \boldsymbol{F_r} \rangle = f_d \boldsymbol{F_r} = f_d(\boldsymbol{f}_g + \boldsymbol{f}_p + \boldsymbol{f}_{\text{drag}} + \boldsymbol{f}_{\text{lift}} + \boldsymbol{f}_{\text{vm}}) \tag{B.15}$$

denoting the gravity, external pressure, drag, lift and virtual mass forces.

Combining all terms gives the equation of change for momentum:

$$\begin{aligned} &\frac{\partial (f_d \boldsymbol{v_r})}{\partial t} + \frac{\partial}{\partial \boldsymbol{r}} \cdot (f_d \boldsymbol{v_r} \boldsymbol{v_r}) + \frac{\partial}{\partial \xi}(f_d v_\xi \boldsymbol{v_r}) \\ &= -\frac{\partial}{\partial \boldsymbol{r}} \boldsymbol{P_r} - \frac{\partial}{\partial \xi} \boldsymbol{p_\xi} + f_d \boldsymbol{F_r} + f_d \langle \frac{\mathrm{d}m_p}{\mathrm{d}t} \frac{\boldsymbol{c}}{m_p} \rangle + \langle S_{\boldsymbol{c}} \rangle \end{aligned} \tag{B.16}$$

Appendix B.4. Enthalpy

To derive the equation of change for molecular temperature one can insert for $\psi_p = h_p$ (Chao, 2012; Lathouwers and Bellan, 2000; Laurent and Massot, 2001; Simonin, 1996) into Eq (23) and re-write the resultant equation of change into temperature by thermodynamical relations. An alternative is to insert for $\psi_p = c_p T_p$ into Eq. (23) directly (Andresen, 1990). It is here chosen $\psi_p = h_p$ where h_p is the bubble enthalpy, dependent on the temperature only. The microscopical heat capacity is assumed constant. This gives:

$$\frac{\partial f_d \langle h_p \rangle}{\partial t} + \frac{\partial}{\partial \boldsymbol{r}} \cdot (f_d \langle \boldsymbol{c} h_p \rangle) + \frac{\partial}{\partial \xi}(f \langle \Xi h_p \rangle) = f_d \langle \frac{\mathrm{d}T_p}{\mathrm{d}t} \frac{\partial h_p}{\partial T_p} \rangle + f_d \langle \frac{\mathrm{d}m_p}{\mathrm{d}t} \frac{h_p}{m_p} \rangle + \langle S_{h_p} \rangle \tag{B.17}$$

818 For the transient term we insert for the mass averaged enthalpy (Eq. (15)):

$$\frac{\partial(f_d\langle h_p\rangle)}{\partial t} = \frac{\partial(f_d h)}{\partial t} \tag{B.18}$$

819 For the convection term in physical space we decompose the enthalpy into a mean
820 and a fluctuating term (Eq. (17)):

$$\begin{aligned}
\frac{\partial}{\partial \boldsymbol{r}} \cdot (f_d\langle \boldsymbol{c} h_p\rangle) &= \frac{\partial}{\partial \boldsymbol{r}} \cdot (f_d\langle (\boldsymbol{v_r} + \boldsymbol{C})(h + h')\rangle) \\
&= \frac{\partial}{\partial \boldsymbol{r}} \cdot (f_d\langle \boldsymbol{v_r}(h + h')\rangle) + \frac{\partial}{\partial \boldsymbol{r}} \cdot (f_d\langle \boldsymbol{C}(h + h')\rangle) \\
&= \frac{\partial}{\partial \boldsymbol{r}} \cdot (f_d \boldsymbol{v_r} h) + \frac{\partial}{\partial \boldsymbol{r}} \cdot (f_d\langle \boldsymbol{C} h'\rangle) \\
&= \frac{\partial}{\partial \boldsymbol{r}} \cdot (f_d \boldsymbol{v_r} h) + \frac{\partial}{\partial \boldsymbol{r}} \cdot \boldsymbol{q_r}
\end{aligned} \tag{B.19}$$

821 where $\boldsymbol{q_r} = f_d\langle \boldsymbol{C} h'\rangle$ (Eq. (19)). For the convective term in property space:

$$\begin{aligned}
\frac{\partial}{\partial \xi}(f_d\langle \Xi h_p\rangle) &= \frac{\partial}{\partial \xi}(f_d\langle (v_\xi + C_\xi)(h + h')\rangle) + \frac{\partial}{\partial \xi}(f_d\langle (v_\xi + C_\xi)(h + h')\rangle) \\
&= \frac{\partial}{\partial \xi}(f_d\langle v_\xi(h + h')\rangle) + \frac{\partial}{\partial \xi}(f_d\langle C_\xi(h + h')\rangle) \\
&= \frac{\partial}{\partial \xi}(f_d v_\xi h) + \frac{\partial}{\partial \xi}(f_d\langle C_\xi h'\rangle) \\
&= \frac{\partial}{\partial \xi}(f_d v_\xi h) + \frac{\partial}{\partial \xi} q_\xi
\end{aligned} \tag{B.20}$$

where $q_\xi = f_d\langle C_\xi h' \rangle$ (Eq. (21)). This gives for the equation of change for enthalpy:

$$\begin{aligned}&\frac{\partial(f_d h)}{\partial t} + \frac{\partial}{\partial \boldsymbol{r}} \cdot (f_d h \boldsymbol{v_r}) + \frac{\partial}{\partial \xi}(f_d v_\xi h) \\ &= -\frac{\partial}{\partial \boldsymbol{r}} \cdot \boldsymbol{q_r} - \frac{\partial}{\partial \xi} q_\xi + f_d\langle \frac{\mathrm{d}T_p}{\mathrm{d}t}\frac{\partial h_p}{\partial T_p}\rangle + f_d\langle \frac{\mathrm{d}m_p}{\mathrm{d}t}\frac{h_p}{m_p}\rangle + \langle S_{h_p}\rangle\end{aligned} \tag{B.21}$$

Appendix B.4.1. Equation of change in terms of temperature

The equation of change for enthalpy (Eq. (B.21)) can be re-written in terms of temperature by use of thermodynamic relations. We subtract continuity (Eq. (24)) from Eq. (B.21) to obtain:

$$\begin{aligned}&f_d\frac{\partial h}{\partial t} + f_d \boldsymbol{v_r} \cdot \frac{\partial h}{\partial \boldsymbol{r}} + f_d v_\xi \frac{\partial h}{\partial \xi} = -\frac{\partial}{\partial \boldsymbol{r}} \cdot \boldsymbol{q_r} - \frac{\partial}{\partial \xi} q_\xi + f_d\langle \frac{\mathrm{d}T_p}{\mathrm{d}t}\frac{\partial h_p}{\partial T_p}\rangle \\ &+ f_d\langle \frac{\mathrm{d}m_p}{\mathrm{d}t}\frac{h_p}{m_p}\rangle - f_d h\langle \frac{\mathrm{d}m_p}{\mathrm{d}t}\frac{1}{m_p}\rangle + \langle S_{h_p}\rangle - h\langle S_1\rangle\end{aligned} \tag{B.22}$$

We first consider the left hand side of Eq. (B.22). The thermodynamical relation for the total derivative of the enthalpy can be given for fluid flow problems as (Jakobsen, 2014):

$$\frac{Dh}{Dt} = C_p\frac{DT}{Dt} + \left(\frac{1}{\rho_G} - T\left[\frac{\partial(\frac{1}{\rho_G})}{\partial T}\right]_{p,\boldsymbol{\omega}}\right)\frac{Dp}{Dt} + \sum_s \left(\frac{\partial h}{\partial \omega_s}\right)_{T,p}\frac{D\omega_s}{Dt} \tag{B.23}$$

where the substantial derivative $\frac{D}{Dt}$ is in the physical space, i.e. $\frac{D}{Dt} = \frac{\partial}{\partial t} + \boldsymbol{v_r} \cdot \frac{\partial}{\partial \boldsymbol{r}}$. In this work we interpret the substantial derivative to include the entire phase

space:

$$\frac{D_a}{D_a t} = \frac{\partial}{\partial t} + \boldsymbol{v_r} \cdot \frac{\partial}{\partial \boldsymbol{r}} + v_\xi \frac{\partial}{\partial \xi} \tag{B.24}$$

This gives for the total derivative of the enthalpy:

$$\frac{D_a h}{D_a t} = C_p \frac{D_a T}{D_a t} + \left(\frac{1}{\rho_G} - T \left[\frac{\partial(\frac{1}{\rho_G})}{\partial T} \right]_{p,\omega} \right) \frac{D_a p}{D_a t} + \sum_s \left(\frac{\partial h}{\partial \omega_s} \right)_{T,p} \frac{D_a \omega_s}{D_a t} \tag{B.25}$$

For an ideal gas we have that $\frac{1}{\rho_G} = \frac{RT}{p\overline{M}_w}$ and can write:

$$\frac{1}{\rho_G} - T \left[\frac{\partial(\frac{1}{\rho_G})}{\partial T} \right]_{p,\omega} = \frac{1}{\rho_G} - T \left[\frac{\partial(\frac{RT}{p\overline{M}_w})}{\partial T} \right]_{p,\omega} = \frac{1}{\rho_G} - \frac{RT}{p\overline{M}_w} = 0 \tag{B.26}$$

This gives for the total derivative of the enthalpy:

$$\frac{D_a h}{D_a t} = C_p \frac{D_a T}{D_a t} + \sum_s \left(\frac{\partial h}{\partial \omega_s} \right)_{T,p} \frac{D_a \omega_s}{D_a t} \tag{B.27}$$

Eq. (B.27) can replace the left hand side of Eq. (B.22).

We then consider the right hand side of Eq. (B.22). For the term $\langle \frac{\mathrm{d}T_p}{\mathrm{d}t} \frac{\partial h_p}{\partial T_p} \rangle$ right hand side of Eq. (B.21) we consider an enthalpy balance for a single bubble. Different models are available in the literature (e.g. Crowe et al. (2011); Haugen et al. (2015); Marchisio and Fox (2013); Seetharaman (2013)). We here chose the model by Lathouwers and Bellan (2001) expressed in terms of temperature as:

$$C_{p,p} \frac{\mathrm{d}T_p}{\mathrm{d}t} = \frac{Q_{cd,p}}{m_p} + \frac{Q_{r,p}}{m_p} + \frac{1}{m_p} \sum_s \frac{\mathrm{d}m_{p,s}}{\mathrm{d}t} (h_v - h_{p,s}) \tag{B.28}$$

where $Q_{cd,p}$ is heat exchanged with the particle through convection and diffusion, $Q_{r,p}$ is the heat exchanged by thermal radiation and $\frac{1}{m_p}\sum_s \frac{\mathrm{d}m_{p,s}}{\mathrm{d}t}(h_v - h_{p,s})$ is the latent heat of vaporization. We can neglect the heat exchange by radiation. Inserting for Eq. (B.28) and Eq. (B.27) into Eq. (B.22) gives the equation of change of enthalpy in terms of temperature:

$$\begin{aligned} &f_d C_p \frac{\partial T}{\partial t} + f_d C_p \boldsymbol{v_r} \frac{\partial T}{\partial \boldsymbol{r}} + f_d C_p v_\xi \frac{\partial T}{\partial \xi} = -\frac{\partial}{\partial \boldsymbol{r}} \cdot \boldsymbol{q_r} - \frac{\partial}{\partial \xi} q_\xi - \sum_s \left(\frac{\partial h}{\partial \omega_s}\right)_{T,p} \frac{D_a \omega_s}{D_a t} \\ &- f_d \langle \frac{Q_{cd,p}}{m_p} \rangle - f_d \langle \frac{1}{m_p} \sum_s \frac{\mathrm{d}m_{p,s}}{\mathrm{d}t}(h_v - h_{p,s}) \rangle + f_d \langle \frac{\mathrm{d}m_p}{\mathrm{d}t} \frac{h_p}{m_p} \rangle - f_d h \langle \frac{\mathrm{d}m_p}{\mathrm{d}t} \frac{1}{m_p} \rangle \\ &+ \langle S_{h_p} \rangle - h \langle S_1 \rangle \end{aligned} \tag{B.29}$$

Appendix C. Implemented equations

This section lists the implemented equations for the demonstration of the model as described in Section 4. The equation of change for total mass is given as:

$$\frac{\partial (f_d(z,\xi) v_z(z,\xi))}{\partial z} + \frac{\partial (f_d(z,\xi) v_\xi(z,\xi))}{\partial \xi} = f_d(z,\xi)\gamma(z,\xi) + S_m(z,\xi) \tag{C.1}$$

where $f_d\gamma$ is a mass transfer term and S_m is the source term due to coalescence and breakage. The boundary conditions are given as:

$$\begin{aligned} f_d|_{z=0} &= f_{d,\mathrm{in}} \\ f_d|_{\xi=\xi_{\min}} &= 0 \end{aligned} \tag{C.2}$$

The growth flux $v_\xi f_d$ is set to zero at the ξ boundaries so that no bubbles enter or leave the domain through growth. The inlet bubble size distribution is calculated by:

$$f_{d,\text{in}} = \frac{A}{\sigma\sqrt{2\pi}}\exp\left[(-(\xi-\overline{\xi})^2/(2\sigma^2))\right] \tag{C.3}$$

where $A = \alpha_{G,\text{in}}\rho_{G,\text{in}}\sigma\sqrt{2\pi}\exp\left[(-(\xi-\overline{\xi})^2/(2\sigma^2))\right]$, $\sigma = 10\times10^{-4}$ and $\overline{\xi} = 10\times10^{-3}$m. The equation of change for species mass is given by:

$$\begin{aligned} &f_d(z,\xi)v_G(z,\xi)\frac{\partial\omega_{G,s}(z,\xi)}{\partial z} + f_d(z,\xi)v_\xi(z,\xi)\frac{\partial\omega_{G,s}(z,\xi)}{\partial\xi} \\ &= \frac{\partial}{\partial z}\left[D_{G,z,\text{eff}}\frac{\partial\omega_{G,s}(z,\xi)}{\partial z}\right] + f_d(z,\xi)\gamma_s(z,\xi) \end{aligned} \tag{C.4}$$

where $f_d\gamma_s$ is the mass transfer term for species s. The boundary conditions are given as:

$$\begin{aligned} &\omega_{G,s}|_{z=0} = \omega_{G,s,\text{in}} \\ &\omega_{G,s}|_{\xi=\xi_{\min}} = K_s\omega_{L,s}(z) \\ &\frac{\partial\omega_{G,s}}{\partial z}|_{z=z_{\max}} = 0 \end{aligned} \tag{C.5}$$

The second boundary condition in Eq. (C.5) implies that the smallest bubbles with diameter $\xi_{\min}$ are assumed to be in gas-vapor equilibrium with the liquid phase at all times. The equation of change for momentum is given by:

$$\begin{aligned} &f_d(z,\xi)v_G(z,\xi)\frac{\partial v_G(z,\xi)}{\partial z} + f_d(z,\xi)v_\xi(z,\xi)\frac{\partial v_G(z,\xi)}{\partial\xi} \\ &= \frac{\partial}{\partial z}\left[\sigma_{G,z,\text{eff}}\frac{\partial v_G(z,\xi)}{\partial z}\right] + f_d(z,\xi)F_{G,z}(z,\xi) \end{aligned} \tag{C.6}$$

with the boundary conditions:

$$\begin{aligned} v_G|_{z=0} &= v_{G,\text{in}} \\ v_G|_{\xi=\xi_{\min}} &= v_L(z) \\ \frac{\partial v_G}{\partial z}|_{z=z_{\max}} &= 0 \end{aligned} \tag{C.7}$$

where the smallest bubbles are assumed to have the same velocity as the liquid. The equation of change for temperature is given by:

$$\begin{aligned} &f_d(z,\xi)C_p(z,\xi)v_G(z,\xi)\frac{\partial T_G(z,\xi)}{\partial z} + f_d(z,\xi)C_p(z,\xi)v_\xi(z,\xi)\frac{\partial T_G(z,\xi)}{\partial \xi} \\ &= \frac{\partial}{\partial z}\left[\lambda_{G,z,\text{eff}}\frac{\partial T_G(z,\xi)}{\partial z}\right] + f_d(z,\xi)q_{G,z}(z,\xi)\rangle \end{aligned} \tag{C.8}$$

where $f_d q_{G,z,c}$ is a heat transfer term. The boundary conditions are given as:

$$\begin{aligned} T_G|_{z=0} &= T_{G,\text{in}} \\ T_G|_{\xi=\xi_{\min}} &= T_{SL}(z) \\ \frac{\partial T_G}{\partial z}|_{z=z_{\max}} &= 0 \end{aligned} \tag{C.9}$$

where the smallest bubbles are assumed to have the same temperature as the slurry.